AGU PUBLICATIONS

JGR

Journal of Geophysical Research: Earth Surface

RESEARCH ARTICLE

10.1002/2013JF002943

Key Points:
- We coupled a 2-D subglacial hydrology model with a 3-D ice dynamics model
- Sliding-opening of cavities is the dominant feedback between ice/water systems
- Evolution of subglacial distributed drainage can look like channelization

Correspondence to:
M. J. Hoffman,
mhoffman@lanl.gov

Citation:
Hoffman, M. J., and S. Price (2014), Feedbacks between coupled subglacial hydrology and glacier dynamics, *J. Geophys. Res. Earth Surf.*, *119*, doi:10.1002/2013JF002943.

Received 5 AUG 2013
Accepted 17 JAN 2014
Accepted article online 20 JAN 2014

Feedbacks between coupled subglacial hydrology and glacier dynamics

Matthew Hoffman[1] and Stephen Price[1]

[1]Fluid Dynamics and Solid Mechanics Group, Los Alamos National Laboratory, Los Alamos, New Mexico, USA

Abstract On most glaciers and ice sheet outlets the majority of motion is due to basal slip, a combination of basal sliding and bed deformation. The importance of basal water in controlling sliding is well established, with increased sliding generally related to high basal water pressure, but the details of the interactions between the ice and water systems has not received much study when there is coupling between the systems. Here we use coupled subglacial hydrology and ice dynamics models within the Community Ice Sheet Model to investigate feedbacks between the ice and water systems. The dominant feedback we find is negative: sliding over bedrock bumps opens additional cavity space, which lowers water pressure and, in turn, sliding. We also find two small positive feedbacks: basal melt increases through frictional heat during sliding, which raises water pressure, and strain softening of basal ice during localized speedup causes cavities to close more quickly and maintain higher water pressures. Our coupled modeling demonstrates that a sustained input of surface water to a distributed drainage system can lead to a speedup event that decays even in the absence of channelization, due to increased capacity of the system through opening of cavities, which is enhanced through the sliding-opening feedback. We find that the negative feedback resulting from sliding-opening is robust across a wide range of parameter values. However, our modeling also argues that subglacial channelization is required to terminate speedup events over timescales that are commensurate with observations of late summer slowdown on mountain glaciers.

1. Introduction

Glaciers move by internal deformation of ice and basal slip, which is composed of sliding of the glacier over its bed and, if present, deformation (or plastic failure) of basal sediments [*Cuffey and Paterson*, 2010]. Basal motion of mountain glaciers is observed to typically be about half of the total motion but is often much higher [*Cuffey and Paterson*, 2010], and similarly, large values have been observed for the Greenland ice sheet [*Lüthi et al.*, 2002; M. Lüthi, personal communication, 2013]. Additionally, changes in water inputs, primarily from surface meltwater penetrating to the bed, cause changes in basal slip, presumably by altering subglacial water pressure or bed contact, both on mountain glaciers [e.g., *Iken and Bindschadler*, 1986; *Mair et al.*, 2002; *Bartholomaus et al.*, 2008] and ice sheets [e.g., *Bartholomew et al.*, 2010; *Hoffman et al.*, 2011]. Despite the primary importance of basal hydrology in controlling glacier flow, the subglacial hydrologic system and its interaction with ice dynamics remain poorly understood [*Clarke*, 2005; *Cuffey and Paterson*, 2010].

In recent years, the importance of including subglacial hydrology and its effect on basal slip in prognostic modeling of ice sheet and glacier evolution has been reemphasized [*Little et al.*, 2007; *Bell*, 2008; *Bartholomaus et al.*, 2008; *Lipscomb et al.*, 2009; *Schoof*, 2010; *Price et al.*, 2011a; *Shannon et al.*, 2013]. During this time, many ice sheet modeling efforts have successfully implemented so-called "higher-order" solutions to the momentum balance for ice flow, which are necessary for accurately simulating a combination of ice deformation and the transfer of stresses that occurs in areas where slip is significant [e.g., *Pattyn et al.*, 2008; *Price et al.*, 2011b; *Larour et al.*, 2012; *Leng et al.*, 2012; *Gillet-Chaulet et al.*, 2012; *Perego et al.*, 2012].

At the same time, substantial progress has been made in realistic modeling of subglacial hydrology. While the importance of subglacial water pressure in modulating glacier sliding has long been recognized, most previous subglacial hydrology models were formulated in terms of the basal water layer thickness, requiring an empirical relation to calculate the subglacial water pressure [e.g., *Alley*, 1989; *Flowers*, 2002a; *Johnson and Fastook*, 2002; *Pimentel and Flowers*, 2010]. Alternatively, the determination of water pressure was avoided altogether and an ad hoc relation linked water layer thickness or flux to sliding rate [e.g., *Le Brocq et al.*, 2009; *Goeller et al.*, 2013]. Other efforts have effectively closed the systems of equations by describing the

evolution of subglacial cavity volume, allowing for water pressure to be solved for directly [e.g., *Kessler and Anderson*, 2004; *Hewitt*, 2011; *Schoof*, 2010].

In addition, while many early models considered only inefficient, distributed drainage (which may be appropriate for environments without surface meltwater inputs to the bed, like Antarctica), later studies combined distributed drainage with efficient, channelized drainage, either as flow line models [e.g., *Flowers*, 2008; *Pimentel and Flowers*, 2010], network models [e.g., *Kessler and Anderson*, 2004], or continuously in two horizontal dimensions [e.g., *Hewitt*, 2011]. Finally, recent work has included spontaneous switching between these two modes of drainage without the need to prescribe the presence of channels [*Schoof*, 2010; *Hewitt*, 2013; *Werder et al.*, 2013], in some cases treating overpressure and underpressure of the hydrologic systems [*Schoof et al.*, 2012; *Hewitt et al.*, 2012].

Tying these two sets of advances together is the formulation of theoretically based friction laws for basal sliding over hard beds that relate subglacial water pressure to basal traction and include the effects of cavitation [*Schoof*, 2005; *Gagliardini et al.*, 2007]. Many previous studies have presented coupled subglacial hydrology and ice dynamics simulations of varying levels of complexity but use empirical or ad hoc sliding relations [e.g., *Johnson and Fastook*, 2002; *Arnold and Sharp*, 2002; *Marshall et al.*, 2005; *Le Brocq et al.*, 2009; *Goeller et al.*, 2013]. Only a handful of recent efforts have also included the more recent improvements in friction laws, in either one (i.e., flowband) [*Pimentel et al.*, 2010; *Pimentel and Flowers*, 2010] or two dimension (i.e., planform) [*Hewitt*, 2013].

The few existing modeling studies that have investigated the coupling between subglacial hydrology and ice dynamics in detail revealed complexities missing from stand-alone studies of either system. *Iken* [1981] found that the effect of water pressure on sliding is not unique and depends on the size of cavities during their transient growth. *Humphrey* [1987] identified the importance of stress-gradient coupling between the ice and water systems which can cause a locally antiphase relationship between water pressure and sliding in a linked-cavity drainage system. These studies highlight the need for more study into the coupled system.

While recent models of coupled subglacial hydrology and ice dynamics do a good job of qualitatively reproducing observed phenomena on mountain glaciers [*Kessler and Anderson*, 2004; *Pimentel et al.*, 2010; *Pimentel and Flowers*, 2010] and ice sheets [*Pimentel and Flowers*, 2010; *Hewitt*, 2013; *van der Wel et al.*, 2013; *Kyrke-Smith et al.*, 2014], it is not yet clear how important feedbacks between the two systems are and under what circumstances; studies focusing only on the hydrologic component have been able to produce water pressure results that qualitatively explain observed spatial and temporal patterns in ice motion [e.g., *Flowers*, 2002b, 2008; *Schoof*, 2010; *Colgan et al.*, 2011; *Bartholomew et al.*, 2012; *Banwell et al.*, 2013; *Werder et al.*, 2013]. Thus, an unresolved question in glaciology is how important the coupling between subglacial hydrology and ice dynamics is on predicting ice motion and under what circumstances this coupling ought to be included in models.

In this work, we investigate feedbacks between subglacial hydrology and ice dynamics for an idealized mountain glacier, using a coupled model of two-dimensional subglacial hydrology and three-dimensional, higher order ice dynamics within the Community Ice Sheet Model [*Price et al.*, 2011b; *Lemieux et al.*, 2011; *Bougamont et al.*, 2011; *Evans et al.*, 2012; *Gladish et al.*, 2012]. We compare differences between a one-way forcing of ice dynamics with the subglacial hydrology model and a full coupling of the two model components so that feedbacks between the two systems can operate. We identify steady state and transient differences in model output between the two approaches following simulated meltwater-induced speedup events, both with and without allowing channelization of the subglacial hydrologic system. Through these experiments and an investigation into parameter sensitivity, we identify where fully coupled treatments are necessary or important, versus where simpler (i.e., one-way forcing) approaches may be adequate. Here we consider only the sliding component of basal slip, ignoring the potential contribution of bed deformation to glacier motion [cf. *van der Wel et al.*, 2013]. While this paper focuses on the coupled model feedbacks, it is motivated by the desire to further understand the full range of possible behaviors that can follow from meltwater-induced speedup.

2. Subglacial Hydrology Model

Subglacial hydrologic systems are typically conceptualized to include a relatively inefficient distributed system, composed of linked cavities formed in the lee of bedrock bumps, porous sediments, or thin films, and

an efficient system of channels melted upward into the base of the ice (see review by *Fountain and Walder* [1998]). While perturbations from externally supplied discharge will increase the water pressure in both types of systems, at steady state water pressure in the distributed system increases with cavity size and discharge, whereas in channels, water pressure decreases with channel size and discharge. When water inputs are low, channels are not sustainable because of increasing creep closure rates with increasing effective pressure (ice overburden pressure minus water pressure). However, when discharge in the distributed system reaches a critical value, channels develop spontaneously due to turbulent heat dissipation; melting of the overlying ice generates more conduit space, allowing for greater discharge and more energy dissipation, which further enlarges a few conduits into concentrated channels.

This conceptual model explains the "spring speedup" that is commonly observed on mountain glaciers [e.g., *Iken et al.*, 1983; *Nienow et al.*, 1998; *Anderson et al.*, 2004]. When surface meltwater first reaches the bed during the melt season, it impinges on a low capacity distributed system that is quickly overwhelmed, elevating water pressures and increasing basal sliding. Sustained meltwater input increases discharge within the distributed system, eventually leading to channelization. As channels evolve during the melt season, the entire system becomes more efficient, lowering water pressures and sliding despite sustained inputs of surface meltwater. A consequence of this seasonal evolution is that ever larger inputs of meltwater are required to sustain or further increase sliding [*Bartholomaus et al.*, 2008; *Schoof*, 2010; *Pimentel and Flowers*, 2010]. A similar increase in drainage efficiency is observed during summer speedup in the ablation zone of the Greenland ice sheet [e.g., *Bartholomew et al.*, 2010; *Hoffman et al.*, 2011], but recent evidence suggests that channelization is delayed or absent inland from the margins where surface slopes, and correspondingly, potential energy for forming channels, are low [*Meierbachtol et al.*, 2013]. Thus, other processes may be contributing to the seasonally increasing efficiency of the subglacial drainage system that is observed there.

The hydrology model we implement contains descriptions for both distributed and channelized drainage and closely follows the formulations of *Hewitt* [2011] with some modifications. The distributed and channel drainage models are coupled to each other through an exchange term and to an ice dynamics model through a Coulomb friction basal friction law [*Schoof*, 2005]. These models are described in further detail below.

2.1. Distributed Drainage

We approximate the distributed drainage component as a macroporous sheet that could describe a variety of diffusive hydrological processes, such as water flow through linked cavities, patchy films, subglacial till canals, or porous subglacial till. Conservation of the mass of water within the two-dimensional sheet is defined by the following:

$$\frac{\partial h}{\partial t} + \nabla \cdot \vec{q} = \frac{m}{\rho_w} + \omega - \gamma \tag{1}$$

where h is the sheet thickness (m), $\vec{q}$ is the areal discharge of the sheet ($m^2\ s^{-1}$), m is the melt rate ($kg\ m^{-2}\ s^{-1}$), ρ_w is the density of water ($kg\ m^{-3}$), ω is an englacial source term ($m\ s^{-1}$) (e.g., water arriving at the bed from a moulin), and γ is water transferred from the sheet to a channel ($m\ s^{-1}$).

A important feature of the hydrology models described by, e.g., *Schoof* [2010], *Hewitt* [2011], and *Schoof et al.* [2012] is the ability to solve for the effective pressure, N, in a macroporous sheet without the need for an empirical formula of the form $N = f(h)$ to close the system of equations [e.g., *Alley*, 1989; *Johnson and Fastook*, 2002; *Flowers*, 2002a]. This is accomplished by including a second equation describing the evolution of cavity space within the sheet:

$$\frac{\partial h}{\partial t} = V_O - V_C \tag{2}$$

where V_O is a sheet opening velocity due to sliding over bumps and V_C is a sheet closing velocity due to creep closure of the ice. For the case where overpressure and underpressure are not considered, water depth and cavity size within the sheet can be assumed equal (i.e., cavities are always considered to be full and smaller than the bump height) which simplifies equation (2) [cf. *Schoof et al.*, 2012].

We allow cavity opening from sliding over bumps:

$$V_O = |\vec{u}_b| \frac{h_r - h}{l_r} \tag{3}$$

where $\vec{u}_b$ is the sliding velocity, and h_r and l_r are parameters describing the height and wavelength, respectively, of bumps on the bed *Schoof et al.* [2012]. While melting can also be included as a process for opening of cavities [e.g., *Hewitt*, 2011], we exclude it here for reasons discussed in the Appendix. It should be emphasized that the representation of bump geometry here is at a subgrid scale and individual bumps are not resolved in the grid geometry used by the model.

We assume a linear relation between effective pressure and creep closure:

$$V_C = \frac{hN}{\eta_i} \tag{4}$$

where η_i is the ice viscosity (Pa s), and N is

$$N = \rho_i g H - P_w. \tag{5}$$

In equation (5), g is the acceleration due to gravity (m s^{-2}), H is ice thickness (m), and P_w is water pressure (Pa). (While a cubic relation between N and V_C [cf. *Schoof et al.*, 2012; *Hewitt*, 2013; *Werder et al.*, 2013] would be more consistent with the constitutive relation we use for ice, such a formulation would lead to a nonlinear partial differential equation in ϕ; for simplicity, we choose the linear relationship [*Hewitt*, 2011].)

It is worth noting that the water pressure and sliding velocity in equation (2) ought to be consistent based on basal friction laws. The hydrology model formulation does not require this, but by coupling to the ice dynamics model, we intend this to be the case (though the friction laws currently available have the restriction that they assume steady state cavity size, which the hydrology model clearly does not).

Closing the equations requires a flow law for $\vec{q}$ and an energy balance for determining the melt rate, m. We use a Darcy style flow law:

$$\vec{q} = -\frac{k_0 h^3}{\eta_w} \nabla \phi_s \tag{6}$$

where k_0 describes the hydraulic transmissivity of the macroporous sheet (dimensionless) and η_w represents the viscosity of water (Pa s). ϕ_s is the hydraulic potential, which is the sum of the pressure associated with the gravitational potential energy at the bed and the water pressure:

$$\phi_s = \rho_w g z_b + P_w = \rho_w g z_b + \rho_i g H - N \tag{7}$$

where z_b is the elevation of the bed (m). Energy for local melting comes from the geothermal flux, G (W m^{-2}), frictional heating from ice sliding, and turbulent dissipation due to water flow. Assuming isothermal ice conditions, this energy is given by the following:

$$mL = G - \vec{u}_b \cdot \vec{\tau}_b - \vec{q} \cdot \nabla \phi_s \tag{8}$$

where $\vec{\tau}_b$ is the basal traction vector and L is the latent heat of fusion of water.

Equation (8) requires careful consideration. Including dissipation in equation (8) and as a mechanism for cavity opening leads to a sheet-flow instability above a critical discharge, q_c, for which dissipation is the same order of magnitude as the passive heating terms [*Walder*, 1986; *Kamb*, 1987; *Schoof*, 2010; *Hewitt*, 2011]. We define a dissipation factor, D_f, which is the ratio of the rate of cavity opening by dissipation to the rate of cavity opening by sliding:

$$D_f = \frac{\frac{\vec{q} \cdot \nabla \phi_s}{\rho_i L}}{|\vec{u}_b| \frac{h_r - h}{l_r}}. \tag{9}$$

When $D_f > 1$, dissipation is the dominant form of cavity opening, which generates a positive feedback leading to channelization. To avoid violating the assumptions of the distributed flow model, which is only valid for $D_f < 1$, we ignore melting and cavity opening resulting from dissipation, eliminating the $\vec{q} \cdot \nabla \phi_s$

term in equation (8). By ignoring dissipation, our model is unable to simulate spontaneous channelization [cf. *Schoof*, 2010; *Hewitt et al.*, 2012; *Hewitt*, 2013; *Werder et al.*, 2013]. Instead, we explicitly include channelized drainage by prescribing the existence of dynamic channels when $D_f \geq 1$ is reached within the model domain. While we consider this as a realistic indicator of when channelization is likely to become important, it is not exact as it does not include the role of closure rate in determining conduit instability [*Schoof*, 2010].

To solve the model for distributed drainage, equations (1) and (2) are combined to form a two-dimensional, linear, elliptic, partial differential equation for ϕ_s. Equation (2) is then used to evolve h in time using a forward Euler time step, which requires keeping time steps small enough to maintain stability.

2.2. Channelized Drainage

Our formulation for channelized drainage describes a Röthlisberger channel [*Röthlisberger and 1972*; *Nye*, 1976], which grows through dissipative heating from the turbulent flow of water and shrinks due to creep closure of the ice roof. We again follow *Hewitt* [2011], defining the mass balance of water within a linear channel as:

$$\frac{\partial S}{\partial t} + \frac{\partial Q}{\partial x} = \frac{M}{\rho_w} + \gamma \Delta x. \tag{10}$$

The evolution of channel area, S (m^2), is given by the following:

$$\frac{\partial S}{\partial t} = \frac{M}{\rho_i} - \frac{S N_c}{\eta_i} \tag{11}$$

where Q is the volumetric channel flow rate ($m^3\ s^{-1}$), N_c is the effective pressure in the channel, and M is the melt rate within the channel ($kg\ m^{-1}\ s^{-1}$). Melt within the channel is entirely from dissipation:

$$ML = Q\frac{\partial \phi_c}{\partial x} \tag{12}$$

where ϕ_c is the hydraulic potential in the channel. Within the channel, we use Manning's law for turbulent flow:

$$FQ^2 = S^{8/3}\frac{\partial \phi_c}{\partial x} \tag{13}$$

where F is a constant taken as 650 $kg\ m^{-8/3}$ [*Hewitt*, 2011].

Similar to solving the distributed system, equations (10) through (13) are combined to form a one-dimensional, nonlinear, elliptic, partial differential equation for ϕ_c, and then equation (11) is used to evolve S in time.

2.3. Hydrology Model Implementation and Numerical Solution

The hydrology model equations are discretized in two horizontal dimensions with finite differences on a C-grid, with scalars (e.g., h, N, ϕ_s) at cell centers and vectors (e.g., $\vec{q}$) at cell edge midpoints. Variables relating to motion and properties of the overlying ice mass ($\vec{u}_b, \vec{\tau}_b,$ and η_i) are obtained through coupling to the ice dynamics model, which we describe further below.

The channel model, initially absent, is prescribed on cell edges when neighboring cells of the distributed drainage system experience $D_f > 1$. The channel is discretized in one-dimension, on cell edges parallel to the x coordinate. The channel begins at the location where the channelization threshold is initially reached and extends downglacier to the terminus. The restriction that the channel lies along cell edges parallel to the x coordinate and the ability to only include a single channel is not a limitation for the idealized experiments presented here but would be inappropriate for more realistic geometric settings. *Werder et al.* [2013] describe a model on an unstructured grid that allows a more natural development of channels for arbitrary geometries, and *Schoof* [2010] and *Hewitt* [2013] describe models that allow channels to develop naturally on structured grids.

The channel model is coupled to the cells of the sheet model on either side by calculating a flux between the channel and the surrounding sheet using the Darcy flow law (equation (6)). In our finite difference discretization, this exchange term, γ, is thus given by the following:

$$\gamma = -\frac{k_0 h^3}{\eta_w} \frac{\phi_c - \phi_s}{\frac{1}{2}\Delta y}. \tag{14}$$

When the channel is added, we prescribe an initial condition of $\phi_c = \phi_s$. This means that initially, there is no exchange between the channel and the surrounding sheet and no "shock" to the distributed drainage system from channel activation. However, to evolve the channel in time requires solving the channel equations for S with known ϕ_c, which results in an initial value problem in the form of a nonlinear, first-order, ordinary differential equation; an infinite set of S profiles can yield the desired initial condition for ϕ_c. To determine a specific solution for the initial profile of S, we use an initial value at the channel initiation site of $S = h^2$. We argue that, to first-order, the area of the channel when it first initiates from the distributed system should be of the same dimension as the sheet thickness. Below, we show that this yields sensible results for incipient channelization, but that the rate of channelization is sensitive to the initial condition on channel area. Models that allow spontaneous channelization [e.g., *Hewitt et al.*, 2012; *Hewitt*, 2013; *Werder et al.*, 2013; *Schoof*, 2010] avoid the need to activate a channel with specified initial conditions but still are sensitive to the initial size of channel elements and the formulation for exchange with the sheet.

3. Ice Dynamics Model

Ice dynamics are modeled with the thermomechanical, three-dimensional, first-order momentum balance solver in the Community Ice Sheet Model (CISM). In a right-handed, Cartesian coordinate system, the first-order momentum balance [*Herterich*, 1987; *Blatter*, 1995; *Pattyn*, 2003; *Dukowicz et al.*, 2010] is given by the following:

$$\frac{\partial}{\partial x}\left(4\eta_i \frac{\partial u}{\partial x} + 2\eta_i \frac{\partial v}{\partial y}\right) + \frac{\partial}{\partial y}\left(\eta_i \frac{\partial u}{\partial y} + \eta_i \frac{\partial v}{\partial x}\right) + \frac{\partial}{\partial z}\left(\eta_i \frac{\partial u}{\partial z}\right) = \rho_i g \frac{\partial s}{\partial x} \tag{15}$$

$$\frac{\partial}{\partial y}\left(4\eta_i \frac{\partial v}{\partial y} + 2\eta_i \frac{\partial u}{\partial x}\right) + \frac{\partial}{\partial x}\left(\eta_i \frac{\partial u}{\partial y} + \eta_i \frac{\partial v}{\partial x}\right) + \frac{\partial}{\partial z}\left(\eta_i \frac{\partial v}{\partial z}\right) = \rho_i g \frac{\partial s}{\partial y} \tag{16}$$

where u and v are the x and y components of velocity, respectively, and s is the glacier surface elevation. The effective ice viscosity, η_i, is a function of the temperature-dependent rate factor A (here taken to be 10^{-16} Pa$^{-\frac{1}{3}}$ yr^{-1} for temperate ice), the second invariant of the strain tensor, $\dot{\epsilon} = \frac{1}{2}(\dot{\epsilon}_{ij}\dot{\epsilon}_{ij})^{1/2}$, and the flow law exponent, n, taken as 3 [*Cuffey and Paterson*, 2010]:

$$\eta_i = \frac{A^{\frac{-1}{n}}}{\sqrt{2}} \dot{\epsilon}^{\frac{1-n}{n}}. \tag{17}$$

The basal boundary condition is a specified basal traction vector, $\vec{\tau}_b = (\tau_{bx}, \tau_{by})$:

$$4\eta_i \frac{\partial u}{\partial x}\frac{\partial b}{\partial x} + \eta_i \frac{\partial u}{\partial y}\frac{\partial b}{\partial y} - \eta_i \frac{\partial u}{\partial z} + 2\eta_i \frac{\partial v}{\partial y}\frac{\partial b}{\partial x} + \eta_i \frac{\partial v}{\partial x}\frac{\partial b}{\partial y} = -\tau_{bx} \tag{18}$$

$$4\eta_i \frac{\partial v}{\partial y}\frac{\partial b}{\partial y} + \eta_i \frac{\partial v}{\partial x}\frac{\partial b}{\partial x} - \eta_i \frac{\partial v}{\partial z} + 2\eta_i \frac{\partial u}{\partial x}\frac{\partial b}{\partial y} + \eta_i \frac{\partial u}{\partial y}\frac{\partial b}{\partial x} = -\tau_{by} \tag{19}$$

where b is the bed elevation and other variables are as given above.

We define basal traction using a physically based basal friction law for sliding over hard beds that allows for cavitation and bounded basal drag [*Schoof*, 2005]:

$$\vec{\tau}_b = C\left(\frac{\vec{u}_b}{\vec{u}_b + N^n \Lambda}\right)^{1/n} N, \Lambda = \frac{\lambda_{\max} A}{m_{\max}}. \tag{20}$$

It has been applied in previous models of coupled hydrology and ice dynamics [*Pimentel et al.*, 2010; *Pimentel and Flowers*, 2010; *Hewitt*, 2013]. In equation (20), C is a Coulomb friction constant, and $\lambda_{\max}$ and

m_{max} are the wavelength (m) and maximum slope, respectively, of the dominant bedrock bumps. Near cavitation (i.e., when effective pressure approaches 0 at high water pressure), the friction law becomes a Coulomb friction law of the form $\tau_b = CN$. Alternatively, at large effective pressures (low water pressure), the friction law takes a power law form, $\tau_b \propto u_b^{1/n}$. As with the hydrology model, the representation of bump geometry in the friction law is at a subgrid scale and not explicitly resolved in the grid geometry used by the model.

The momentum balance is discretized using finite differences on a B-grid with scalars (e.g., H, s, and b) at cell centers and vectors (e.g., u and v) on a staggered grid at vertices. Nonlinearity in the equations associated with the effective viscosity is treated with either a Picard or Jacobian-Free-Newton-Krylov fixed-point iteration. Additional discussion of the ice dynamics model and solution procedures are given in *Price et al.* [2011b], *Lemieux et al.* [2011], and *Evans et al.* [2012].

The ice dynamics and hydrology model components share the same regular grid and the same time step (both use forward Euler time discretization). While it is possible to use different time steps between the two models and it may be impractical to keep them equal for long simulations, in this study we keep them equal to study the coupled system in full detail.

Because our experiments are at the seasonal time scale, we assume a fixed geometry and only use CISM's capability for diagnostic solutions of ice velocity. This is equivalent to assuming negligible ice thickness change over the length of a season. The ice dynamics model component receives the effective pressure in the distributed drainage system, N, from the hydrology model in order to solve equations (18) and (19) using equation (20). There is no direct coupling between the ice dynamics and the channel, because the channel is assumed to be infinitely thin and the important aspect of the coupling is how it lowers water pressure in the distributed drainage system. Because of the two-way communication between hydrology and ice dynamics, a fixed-point iteration (Picard) of the time-independent solutions of u, v (and associated τ_{bx}, τ_{by}, η_i) and N is required to make the solution of the hydrologic and ice dynamic states consistent at each time step (this is different than obtaining a steady state solution). This occurs in addition to the fixed-point iteration used in the ice dynamics model to deal with the nonlinearity in effective ice viscosity when solving equations (15)–(16) and the fixed-point iteration used in the hydrology model to obtain consistency between ϕ_s and ϕ_c.

4. Experiments

To investigate feedbacks in the coupled hydrology-ice dynamics system, we run a series of increasingly complex experiments, using an idealized mountain glacier geometry. With a single chosen set of parameters, we first explore the effects of the various couplings in detail. This is followed by a more general assessment of the sensitivity of the feedbacks to a range of parameter values.

The coupled model has both positive and negative feedbacks between sliding and the distributed hydrologic system. Sliding over bedrock bumps opens additional cavity space (equation (3)), which lowers water pressure and, in turn, sliding, generating a negative feedback. Sliding also provides frictional heat for basal melt (equation (8)). In our model formulation, a source of water from basal melt increases water pressure, forming a feedback that is positive but typically much smaller in magnitude than the negative feedback associated with cavity opening from sliding. However, if cavities in the distributed hydrologic system are allowed to open through basal melting, this process results in a small negative feedback (Appendix). Finally, strain softening of the ice near the bed during localized, meltwater-induced speedup forms a negative feedback; softening causes cavities to close more quickly (equation (4)), maintaining higher water pressures, and enhancing sliding. All of these feedbacks are demonstrated through model simulations and discussed in greater detail below.

4.1. Coupling Configurations

To illustrate these feedbacks, we perform a series of model runs with different degrees of coupling between the hydrology and ice dynamics model components. We first spin up the coupled hydrology and ice dynamics model to a steady state using the fixed glacier geometry and no external forcing ($\omega = 0$). We then initiate a meltwater-induced speedup event by applying a steady input of water to a single location of the subglacial hydrologic system (i.e., activating a moulin). We model the resulting pressurization and speedup under four scenarios. In all scenarios, the ice dynamics model component uses transient modeled values of

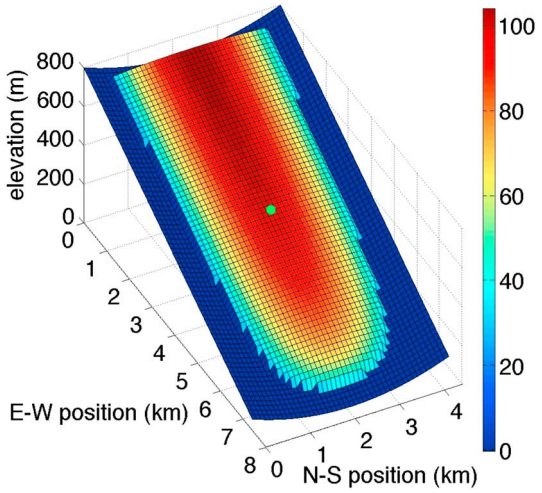

Figure 1. Idealized mountain glacier test case geometry. Colors indicate ice thickness. Green dot is moulin location for meltwater-induced speedup experiments.

effective pressure (N) to drive sliding. No channel is present initially, but in some simulations, we allow for and explore channelization when $D_f \geq 1$ during the simulation, as discussed below. The model is run for 1 year with a time step of 0.01 yr for all model components. For stability, smaller time steps are used when the channel is also present.

The different coupling configurations are the following:

1. *One-way forcing (run 1N)*. The hydrology model assumes prescribed sliding velocity ($\vec{u}_b$), basal traction ($\vec{\tau}_b$), and effective ice viscosity (η_i) fields in equations (3), (4), and (8), which are taken from the steady state initial condition and held fixed throughout the simulation. However, the ice dynamics model receives and uses updated fields of effective pressure (N) from the hydrology model for use in the friction law (equation (20)). This is a control run where the coupling is in only one direction, from the hydrology model to the ice dynamics model.
2. *Two-way coupling of sliding (run 2S)*. The hydrology model takes modeled temporally and spatially varying fields of sliding velocity ($\vec{u}_b$) and basal traction ($\vec{\tau}_b$) during the simulation, but the steady state initial condition for effective ice viscosity (η_i) is prescribed and held fixed within the hydrology model throughout the simulation. The ice dynamics model applies updated values for effective pressure (N) in its basal friction law. This configuration illustrates the feedbacks related to sliding only.
3. *Two-way coupling of viscosity (run 2V)*. The hydrology model takes the steady state, initial sliding speed ($\vec{u}_b$) and basal traction ($\vec{\tau}_b$) and holds them fixed throughout the simulation but updates the hydrology model with temporally and spatially varying fields of effective ice viscosity (η_i). The ice dynamics model applies updated values for effective pressure (N) in its basal friction law. This configuration illustrates the (positive) feedback related to only the softening of ice during speedup.
4. *Two-way, fully coupled (run 2F)*. The hydrology model takes modeled temporally and spatially varying fields of sliding velocity ($\vec{u}_b$), basal traction ($\vec{\tau}_b$), and effective ice viscosity (η_i) from the ice dynamics model, and the ice dynamics model applies updated values for effective pressure (N) in its basal friction law. This configuration illustrates full coupling of the two models, using internally consistent coupling fields, and demonstrates the full range of interactions between the various positive and negative feedbacks.

4.2. Test Case

The geometry for our test case represents an idealized mountain glacier having a centerline longitudinal profile consistent with a plastic rheology [*Schoof et al.*, 2012; *Nye*, 1951] and resting in an inclined trough. The centerline longitudinal profile of the upper surface, $s(x, 0)$, is described by the following:

$$-\rho_i g(s-b)\frac{\partial s}{\partial x} = \tau_c \tag{21}$$

where the glacier bed elevation is $b(x, 0) = -b_0(1 - x/x_m)$, with $b_0 = 700$ m, $x_m = 7000$ m, and $\tau_c = 10^5$ Pa. The glacier surface and bed have parabolic transverse profiles of the form $b(x, y) = b(x, 0) + 2.0 \times 10^{-5}y^2$ and $s(x, y) = s(x, 0) + 0.5 \times 10^{-5}y^2$, respectively. The resulting geometry is 7 km long and 3.5 km wide with a typical thickness of ~100 m (Figure 1). We use a horizontal grid cell size of 100 m with 10 vertical levels for the ice dynamics calculation. We ignore effects originating from parts of the glacier upstream of the $x = 0$ domain boundary and apply $P_w = 0$ Dirichlet boundary conditions along all glacier margins [*Flowers*, 2002b]. While we considered no-flux boundary conditions along the lateral and upglacier boundaries, they lead to regions of underpressure ($P_w < 0$ or partially filled cavities), which our model does not treat realistically. The results discussed below are largely insensitive to the choice of hydrology boundary condition. The ice dynamics lateral boundary condition is Dirichlet zero velocity. This boundary condition affects sliding velocities and, in turn, cavity opening within a few ice thicknesses of the margins, but effects are negligible in the center of the domain where we focus our study.

Table 1. List of Physical Constants and Model Parameters[a]

	Definition	Value
	Physical Constants	
ρ_w	density of water	1000 kg m^{-3}
ρ_i	density of ice	900 kg m^{-3}
g	gravitational acceleration	9.81 m s^{-2}
L	latent heat of fusion of water	3×10^5 J kg^{-1}
η_w	viscosity of water	10^{-3} Pa s
	Hydrology Parameters	
h_r	height of bedrock bumps	[0.05 m]
l_r	wavelength of bedrock bumps	[2 m]
G	geothermal heat flux	0.06 W m^{-2}
k_0	dimensionless transmissivity coefficient	10^{-6}
	Ice Dynamics Parameters	
A	flow law parameter	1.0×10^{-16} Pa^{-3} yr^{-1}
C	Coulomb friction coefficient	[0.25]
λ_{max}/m_{max}	ratio of controlling bedrock bump wavelength to maximum slope	[1.5 m]

[a]Brackets indicate values used only for the primary set of experiments discussed in sections 5.1–5.3.

4.3. Parameter Choices

The standard set of parameter values used for the runs described above and discussed in sections 5.1–5.3 are given in Table 1. We consider h_r, l_r, and k_0 to be unknown, site-specific parameters for the hydrologic system and C and $\lambda_{\max}/m_{\max}$ similarly for the basal friction law. All other parameters are chosen to be representative of a temperate glacier (e.g., G and A). The hydrology parameter values were chosen to be similar to those applied in previous studies using similar hydrology models [e.g., *Hewitt*, 2011; *Schoof et al.*, 2012]. The friction law parameter values were chosen to give velocities of order 10^1 m yr^{-1} at steady state. The moulin input used during the meltwater-induced speedup experiments is 0.073 m^3 s^{-1}, which is roughly the runoff from a 0.5 $\times$ 0.5 km region melting at a rate of 2.5 cm d^{-1}.

To investigate the sensitivity of the coupled feedbacks to a range of parameter values, we perform an additional series of model runs comparing the fully coupled and uncoupled models (sections 5.4–5.5). These runs investigate only distributed drainage evolution and do not include the channel model. Keeping the basal friction law parameters fixed to the values from the base case, we vary two of the hydrology model parameters, for an additional 68 runs (h_r=0.03–0.11 m and l_r=0.25–7.5 m). Then, keeping the hydrology parameters fixed to the values from the base case, we vary the two friction law parameters, for an additional 108 runs ($\frac{\lambda_{\max}}{m_{\max}}$ = 0.25–4.0 m, C = 0.175–0.5). While a defensible argument could be made for linking the bed roughness parameters from the hydrology model and the friction law, doing so requires making assumptions about the shape of bed roughness features. To keep our parameter sensitivity analysis general, we have refrained from doing so, with the primary goal of assessing the robustness of the results shown for the base case.

5. Experimental Results and Analysis

5.1. Initial Condition

Figure 2 shows the results of the steady state spin-up for the coupled hydrology and ice dynamics model components. The water layer thickness in the distributed hydrologic system and the eastward water flux both increase moving downglacier, as expected. Values are lower near the lateral margins and water is preferentially routed through the center of the bed trough. The steady state water pressure is greatest in the center of the glacier where ice is thickest. The spatial pattern of sliding speed is roughly similar, with high water pressures generating high rates of sliding. Basal traction is largest where the ice is thickest. The effective viscosity of the basal layer of ice is ~1 MPa yr over much of the glacier but is higher near the margins, where strain rates are relatively smaller.

In experiments conducted using stand-alone hydrology models, by necessity it is common to specify the values for $\vec{u}_b$, $\vec{\tau}_b$, and η_i. Often these are prescribed as fixed and spatially uniform, since an ice dynamics model is not available for generating more realistic fields. To assess the errors introduced by such an approach, we

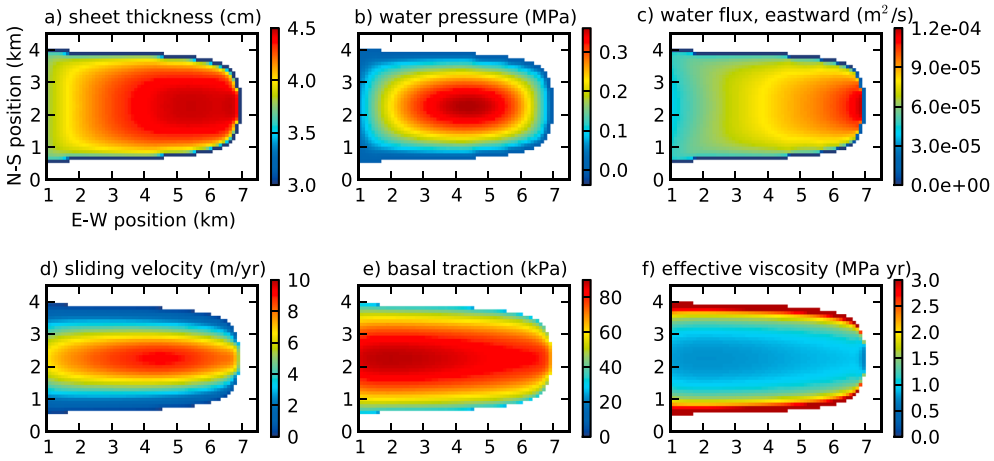

Figure 2. Spun-up initial conditions for the coupled model. Hydrology fields: (a) sheet thickness, (b) water pressure, and (c) eastward water flux. Ice dynamics fields: (d) sliding speed, (e) basal traction, and (f) basal ice effective viscosity.

compare the coupled model results from Figure 2 with results obtained when running our hydrology model component to steady state but using spatially uniform ice dynamics fields, which are calculated from spatial averages of the fields in Figure 2. Specifically, we calculate error, E, at each grid cell as

$$E = \frac{F_{\text{avg}} - F_{\text{cpl}}}{F_{\text{cpl}}} \tag{22}$$

where F_{avg} is the value of a field spun-up using spatially uniform ice dynamics fields and F_{cpl} is the value using the coupled spin-up.

Figure 3 shows the errors associated with assuming spatially uniform ice dynamics forcing relative to our fully coupled spin-up. When spatially uniform ice dynamics fields are assumed, the water layer thickness of the distributed hydrologic system is too thick along the lateral margins and too thin in the center of the glacier because the large lateral gradients in sliding velocity are missing (Figure 2d), and therefore, the associated gradients in cavity opening are absent. The eastward water flux shows a similar pattern due to its strong dependence on water layer thickness (equation (6)). Water pressure is too low near the margin, but too high over most of the glacier, in some places by more than 50%. If this water pressure field was used to calculate a velocity field, the velocity would be ~13% too large (Figure 3d). Thus, for this test case, the errors associated with assuming ice dynamics fields that are (unrealistically) spatially uniform can be locally large but only represent a minor bias when averaged over the domain.

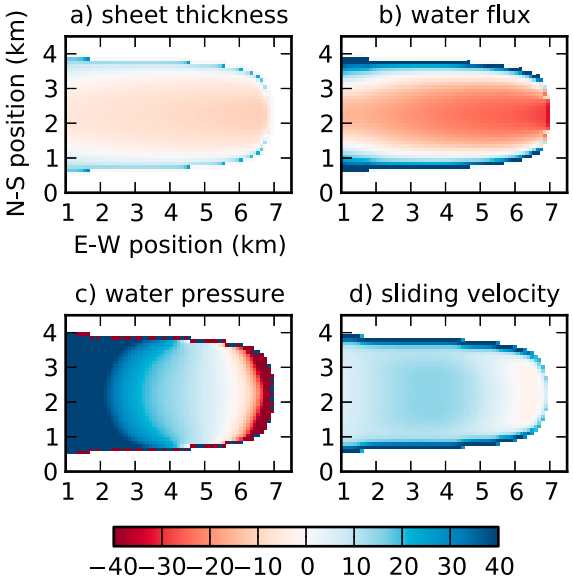

Figure 3. Percent error in model results from spin-up with spatially uniform ice dynamics relative to spin-up with coupled hydrology and ice dynamics for (a) water layer thickness, (b) x direction water flux, (c) water pressure, and (d) sliding velocity.

5.2. Coupled Response of Distributed Drainage Model to Meltwater-Induced Speedup

When input from a moulin is added to the initial state of the distributed model and no channels are allowed to form, there is a large increase in sliding at the moulin site followed by a gradual lowering (Figure 4). Importantly, both the transient response and the new steady state with the steady moulin input differ significantly depending on the level of coupling between the hydrology and ice dynamics

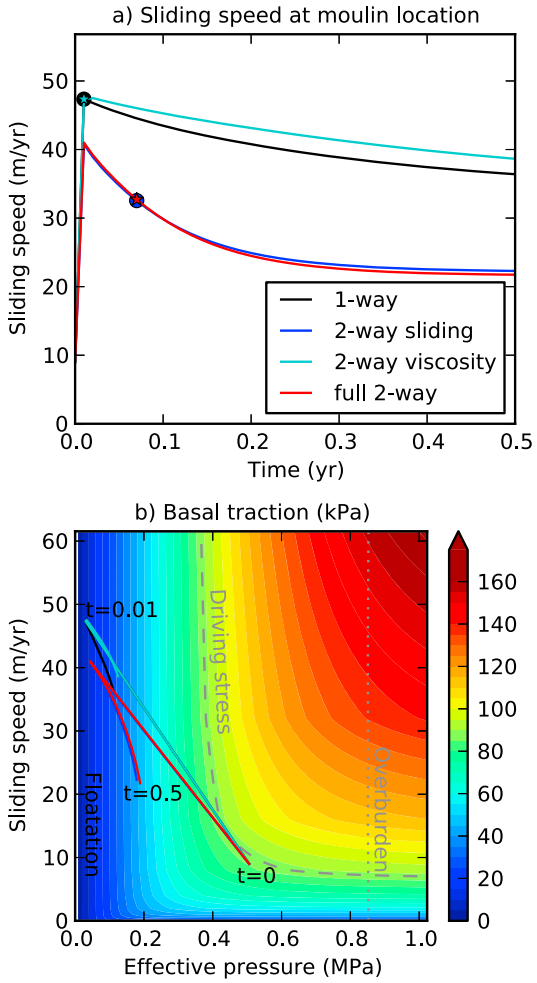

Figure 4. (a) Sliding speed at moulin location during meltwater-induced speedup experiment for various levels of coupling: one-way (1N, black), two-way sliding (2S, blue), one-way viscosity (2V, cyan), and full two-way (2F, red). The circle/star symbols indicate when channelization initiates. (b) Basal traction at moulin location during meltwater-induced speedup event, line colors as in Figure 4a.

model. With one-way forcing (run 1N, black line), the initial sliding speedup is large (5.2×) and the subsequent reduction in sliding is relatively slow (23% reduction in half a year). When sliding alone is coupled with hydrology (run 2S, dark blue line), the initial speedup is less (4.6×) and the subsequent reduction in speed occurs more rapidly (47% reduction in half a year), as a result of lowering water pressures associated with increased cavity opening. If effective ice viscosity alone is coupled (run 2V, light blue line), the initial speedup is similar to the one-way forcing case, but the subsequent reduction in speed occurs more slowly (18% reduction in half a year), and there even is a brief increase in speed during the first time step following the initial speedup. This speedup results from an increase in water pressure due to increased creep closure relative to the case when coupling with effective viscosity is ignored. When both sliding and viscosity are coupled (run 2F, red line), the response is very similar to the case when only sliding is coupled, indicating that the positive feedback associated with viscosity is less important than the negative feedback associated with sliding.

The role of velocity coupling is clear from a snapshot of the model state at time 0.05 year, shown in Figure 5. In the coupled case, cavity space opens at a faster rate during the speedup event due to the increased sliding speed (Figures 5f and 5g). In the uncoupled case, the opening rate remains constant throughout the simulation (Figure 5c). The extra storage capacity provided by the faster opening rate in the coupled case (Figure 5h) allows the distributed system to better accommodate the additional water input, reducing the water pressure relative to the uncoupled case (Figures 5e and 5a). In turn, the lower water pressure results in relatively slower sliding (Figures 5f and 5b).

Prior to the meltwater-induced speedup event, the basal traction at the moulin location nearly balanced the driving stress (Figure 4b). Effective pressure near the moulin was large enough for this location to reside in the nonlinear, viscous drag region of the basal friction law parameter space (where basal traction is insensitive to small changes in effective pressure) (t = 0 in Figure 4b). The addition of meltwater lowered effective pressure to nearly zero (floatation), bringing this location into the Coulomb friction region of friction law parameter space (t = 0.01 in Figure 4b). Because basal traction is proportional to effective pressure in this region, basal traction also approaches zero when the meltwater input is initiated. The difference in transient response between the uncoupled and fully coupled runs can be seen in the recovery curves (t = 0.01–0.05 in Figure 4b); effective pressure increases more and at a faster rate in the fully coupled case (red), resulting in greater basal traction and therefore lower velocity than in the uncoupled case (black).

The spatial pattern of stress redistribution during the speedup event for the two model runs can be seen in the snapshot of the model states at time 0.05 yr (contours in Figures 5b and 5f). In both cases, it can be seen that basal traction is a very small fraction of local driving stress near the moulin location, but in the fully coupled run, the basal traction is already about 20% larger at this time than in the uncoupled run. In both runs, the area experiencing lowered basal traction mirrors the water pressure field and is broad and extends

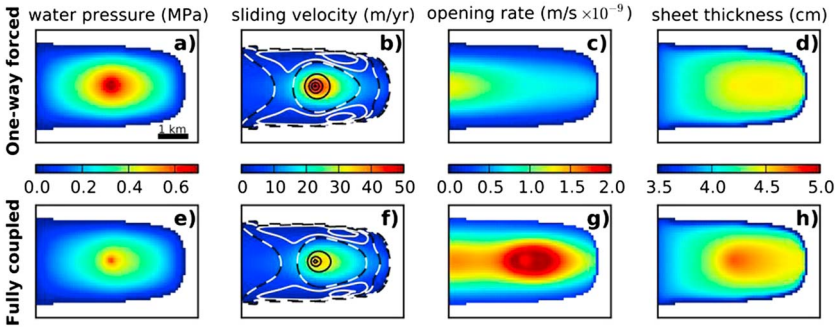

Figure 5. Comparison of (a and e) water pressure, (b and f) sliding velocity, (c and g) sheet opening rate, and (d and h) sheet thickness at time 0.05 yr for one-way forcing (run 1N, Figures 5a–5d) and full coupling (run 2F, Figures 5e–5h) using distributed drainage only. Contours in Figures 5b and 5f show the ratio of the basal traction to the driving stress expressed as a percentage. The black/white dashed line is 100%. The black lines are contours at −20% intervals and indicate regions where basal traction is smaller than driving stress. The white lines are contours at +2% intervals and indicate regions where basal traction is larger than driving stress.

preferentially downglacier. Stress transfer primarily occurs to the lateral margins, as modeled for (soft-bedded) Black Rapids Glacier, Alaska [*Truffer et al.*, 2001; *Amundson et al.*, 2006]. Gradients in effective pressure are larger in this direction than in the longitudinal direction. The increase in drag along the lateral margins is of a much smaller magnitude than that of the decrease near the moulin, but it is spread over a larger area, demonstrating how a local change in traction can have a wide effect. It should be pointed out that the speedup event causes elevated sliding and deformation in the regions where basal traction becomes substantially larger than the local driving stress, highlighting the hazard of treating those two components of ice motion independently [*Truffer et al.*, 2001]. Finally, we note that in the fully coupled case, the extent and magnitude of the region with elevated basal drag is slightly reduced relative to the uncoupled case.

5.3. Coupled Response of Distributed and Channelized Drainage Model to Meltwater-Induced Speedup

When channels are allowed to form during the speedup event, the speedup terminates more quickly (Figure 6a). In the uncoupled case (run 1N, black lines), the channelization threshold ($D_f \geq 1$) is reached as soon as the moulin is activated. However, in the fully coupled case (run 2F, red lines) the channelization threshold is not reached until 0.07 yr because the initial hydropotential gradients (and therefore the turbulent dissipation) are much lower. D_f reaches 1 only after the distributed system has evolved to a point where the water layer thickness and, in turn, the water flux are large.

Once channelization begins, the immediate response of the model with the channel included (dashed lines in Figure 6a) is identical to the model without the channel (for both 1N and 2F runs). The responses quickly diverge due to the influence of the channel, as expected, and the continuous nature of both the sliding speed and its time derivative when the channel is activated giving confidence in our choice of channel initial conditions. To assess the sensitivity of channelization to the channel initial conditions, we also perform runs with the fully coupled model (2F) where the channel initial area is an order of magnitude larger and smaller (we maintain the requirement of no exchange between the channel and distributed system at channel initiation; see discussion in section 2.3). If the initial channel area is too small (upper red dotted line in Figure 6a), the presence of the channel has a negligible effect on the distributed system (and ice dynamics) for a long period of time (>0.2 yr). If the initial channel area is too large (lower red dotted line in Figure 6a), it takes large volumes of water from the sheet too quickly, resulting in a shock to the distributed hydrologic system and a nonphysical discontinuity in the slope of effective pressure and sliding speed. Clearly, using the distributed system layer thickness to estimate the initial area of the channel provides the most physically realistic result.

Some time (~0.05 yr for the 2F run) is required for the channel to grow large enough to markedly affect the water pressure in the distributed system and, in turn, the sliding speed (dashed lines in Figure 6a). Initially, as prescribed, there is no influx to the channel from the sheet, but by 0.12 year in the fully coupled model (run 2F), there is small inflow to the channel near the moulin, outflow back to the sheet at around the 5 km location where the channel area remains small, and inflow to the channel again near the terminus of the glacier (Figures 7a and 7c). Between 0.16 and 0.18 years the channel grows markedly (Figure 7a) resulting

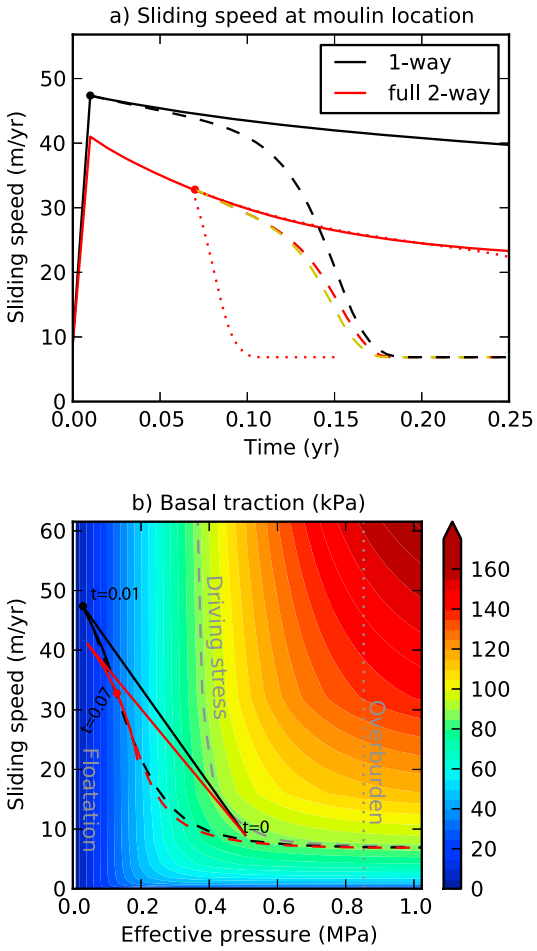

Figure 6. (a) Sliding speed at moulin location during meltwater-induced speedup experiment including effects of channelization for one-way forcing (1N, black) and full two-way coupling (2F, red). The dot symbols indicate when channelization initiates. Solid lines are results without allowing channelization and dashed lines are results allowing channelization. Red dotted lines indicate results when the channel initial area is an order of magnitude smaller (upper dotted line) or larger (lower dotted line) than the square of the sheet thickness. For the yellow line, ice dynamics forcing of the hydrologic system is held constant to the values at channelization initiation (0.07 yr). (b) Basal traction at moulin location during meltwater-induced speedup event, with line colors and styles as in Figure 6a.

in an increase in effective pressure (Figure 7b) and inflow from the sheet (Figure 7c) along the length of the channel. Notably, during this time the constriction in channel area near the 5 km location is eliminated (Figure 7a). Once the channel capacity is large enough to capture a substantial volume of water from the moulin (20% by time 0.18 year), the water pressure in the distributed system and the sliding speed reduce rapidly (Figure 6a). The peak rate of slowdown with the channel in the fully coupled model (2F) is over 3 times faster than without a channel present, and the new steady state speed at the moulin is much lower with the channel present (Figure 6a).

The final speed with channelization included is the same for the uncoupled (1N) and fully coupled (2F) models. This is a consequence of the basal friction law; in both runs the final effective pressure is large enough so that basal traction becomes independent of effective pressure and any further changes to the hydrologic state do not affect the ice dynamics (Figure 6b). Though the uncoupled and coupled runs with channelization have the same final speed, the transient is quite different. The uncoupled run reaches the final speed at approximately the same time as the coupled run, but the uncoupled run maintains faster sliding speeds for a longer period. The concurrent timing of attaining the new steady state velocity for the two runs appears to be coincidental, and, in any case, the integrated displacement from initial speedup to new steady state for the one-way forced run is 31% farther than for the two-way coupled run. The relatively slow evolution of the channel for the first ~0.05 year in the one-way coupled run is due to the fact that the sheet thickness (which is used as the initial condition for the channel) is still relatively small at time 0.01 year; by the time the channel initiates in the two-way coupled run (0.07 year), the sheet has evolved to a larger depth, so the initial channel is substantially larger and therefore more efficient. Importantly, in the coupled run a substantial fraction of the total slowdown (25%) and the total duration of transient response (35%) are due to evolution of the distributed system prior to the onset of channelization. Thus, even when channelization controls the ultimate evolution of the hydrologic system, the dynamics of the distributed system can contribute an important component of evolution prior to channelization.

To assess if the feedbacks between hydrology and ice dynamics are important during channelization, we perform an additional run where the ice dynamics forcing for the hydrology model component is held constant to the values from time 0.07 year when channelization is initiated. As expected, the resulting velocity (yellow dashed line) is less than if the system had remained fully coupled (red dashed line) because sliding opening of the distributed hydrologic system remains at an elevated rate. However, the

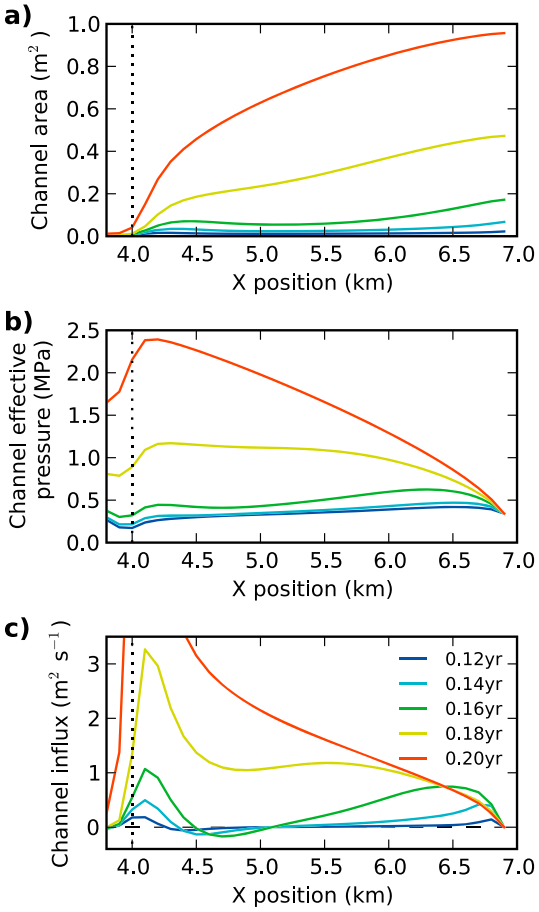

Figure 7. Profiles of the channel characteristics in the fully coupled model (2F) for select times, showing evolution of (a) channel area, (b) effective pressure in the channel, and (c) influx from the sheet to the channel. Dotted line shows location of moulin. The vertical scale in Figure 7c is reduced to show detail at early times; the maximum influx at time 0.20 year is 7.6 m^2 s^{-1}.

difference is slight, and it appears that forcing of the distributed hydrologic system from an evolving channel dominates over forcing from changes in ice dynamics.

5.4. Parameter Sensitivity of Coupled Feedbacks - Hydrology Parameters

The results presented in the previous sections show strong feedbacks between the distributed drainage system and ice dynamics when channelization is not included (or before it begins); the fully coupled model (2F) exhibited a speedup that was 87% of that from the one-way forced model (1N) at the time the moulin was activated and was ~60% as large during most of the 1 year simulation (Figure 4). To assess how changes in the default parameter values affect the strength of the modeled feedbacks, we ran the coupled (2F) and one-way forced (1N) hydrology and ice dynamics model components with no channelization for a range of parameter values.

For each parameter combination, we determine the meltwater input rate required to generate a 4.55× speedup with the coupled (2F) model (in order to match the relative speedup of the coupled run for the base case and provide a basis for comparing results with different parameter values). Then that meltwater input rate is used to force both the coupled (2F) and one-way forced (1N) models for 1 year. Figures 8–9 show that the feedbacks discussed above for the default parameters also exist for a wide range of parameter values. We assess the strength of the feedbacks over the course of each run by calculating a "speedup ratio" at each time step, defined here as the ratio of speedup from the fully coupled model to the one-way forced model—values less than 1.0 indicate net negative feedback in the coupled model.

Figure 8 shows the speedup ratio for variations of the two hydrology model parameters, h_r and l_r, the bump height and wavelength. As seen in the previous example (Figure 4), the feedback strength is relatively weak when the moulin is first activated (Figure 8a), substantially stronger when the system is reaching a new steady state (Figure 8b), and strongest at intermediate times (Figure 8c). The strongest feedbacks are seen for small values of h_r, but strong feedbacks are seen after the initial time for the entire range of h_r values sampled and for l_r values greater than ~1 m. Small values of l_r exhibit weak negative feedbacks at all times of the simulations.

For large h_r values (right of black dashed line), the distributed system flux for the initial condition (steady state spinup) is large enough that channelization should occur somewhere in the model domain prior to the initiation of the meltwater-induced speedup event. Because we do not include channels in these parameter sensitivity experiments, feedback strength is likely overestimated in this region, particularly with increasing distance to the right of this threshold. The relatively small values of h_r at which channelization is triggered during spinup is largely a consequence of the cubic dependence of sheet thickness in the distributed drainage flux law that we use (equation (6)); other parametrizations of distributed drainage flux could allow larger bump heights without channelization. Additionally, for large l_r values (above the white dashed line),

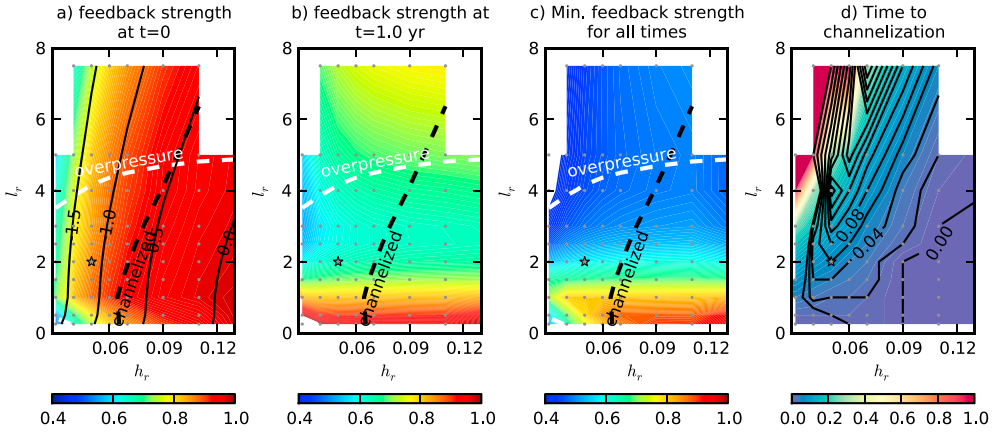

Figure 8. Sensitivity of coupled feedback strength to hydrology parameters, h_r and l_r. All results use meltwater input required to generate a speedup of 4.55× at the moulin location with the coupled (2F) model (without channel model included). (a) Speedup ratio (ratio of coupled model speedup to that from the uncoupled model) at time of moulin activation. Thin black lines are contours of the log of meltwater input ($m^3\ s^{-1}$) required to achieve 4.55× speedup. To the right of the black dashed line, the channelization threshold has been surpassed within the model domain at the initial time prior to moulin activation. Above the white dashed line, overpressure occurs at moulin location at the time of moulin activation. Gray dots indicate parameter values sampled, and the star is the parameter combination discussed in detail in sections 5.1–5.3. (b) Speedup ratio at time 1.0 year, which is close to steady state for most parameter combinations. (c) Minimum value of speedup ratio for all times. (d) Time (year) past moulin activation at which channelization threshold is surpassed near the moulin for the coupled model (colors). The black lines show contours of additional time to channelization for the coupled model relative to the uncoupled model.

overpressure ($N < 0$) occurs near the moulin when it is activated. Because our model does not robustly treat overpressure, results in this region may also be inaccurate, although the spatial extent of overpressure within the model domain is small and unlikely to substantially affect the results in most of the overpressure region shown. Overpressure occurs easily in this region because a large bump wavelength results in a relatively small amount of cavity opening (equation (3)).

The large feedback strength (speedup ratio $\ll 1.0$) at the initial time of moulin activation when h_r is small (Figure 8a) is related to the small water inputs required to pressurize the distributed system when the bump height, and therefore the overall capacity of the system, is small. This can be seen by the close correspondence between contours in meltwater input and contours in feedback strength (Figure 8a). This situation makes changes in the ability of the system to accommodate water (changes in cavity opening from an increase in sliding speed) large relative to the source of water being added (the moulin input), which means

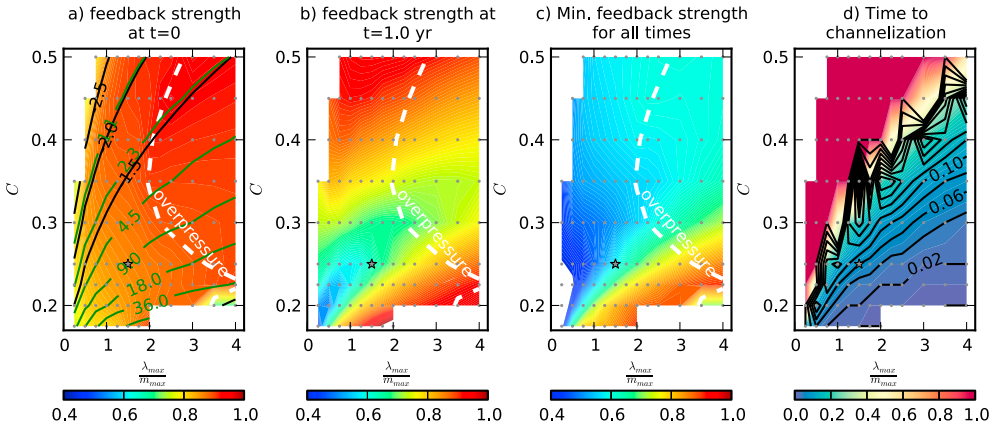

Figure 9. Sensitivity of coupled feedback strength to basal friction law parameters, C and $\frac{\lambda_{max}}{m_{max}}$. All runs model a meltwater-induced sliding speedup of 4.55× at the moulin location without the channel model. Aside from parameters sampled, the plot descriptions are the same as for Figure 8. Additionally, selected contours of initial sliding speed at moulin location (m yr^{-1}) are shown in green in Figure 9a.

that coupling between ice dynamics and hydrology will yield substantially different results than when ignoring coupling.

When the moulin is first activated, feedback strength is controlled entirely by how the instantaneous changes in ice dynamics affect the calculation of hydropotential (i.e., water pressure). At subsequent times feedback strength is also affected by differences in evolution of the distributed drainage system affected by the coupling. This explains why the patterns of parameter sensitivity at later times (Figures 8b–8c) are very different than when the moulin is first activated (Figure 8a). At later times, feedback strength is fairly uniformly large when $l_r > \sim 2$ m. When bump wavelength is small ($l_r < \sim 2$ m), cavities are nearly at their maximum size at the initial state, and, therefore, opening rates and associated evolution of the capacity of the distributed system are limited (whether the model is coupled or not), resulting in little difference between the two models. Finally, it should be noted that feedback strength does not monotonically increase in any direction, and other processes may be dominant in regions beyond those described here.

Although this parameter sensitivity analysis demonstrates that coupled feedbacks are important for a wide range of parameter values, section 5.3 showed that once channelization occurs, feedbacks between hydrology and ice dynamics become substantially less important. Thus, the importance of these feedbacks depends on the duration over which they are able to act prior to the onset of channelization. Figure 8d shows the time until the onset of channelization for the coupled model and how much additional time the coupled model remains unchannelized relative to the uncoupled model. Small h_r is most favorable to long times until channelization because of the cubic dependence on h in the distributed drainage flow law. Over most of the parameter space sampled, time until channelization with the coupled model is 0.02–0.2 year, and for some parameter combinations, channelization does not occur at all. Importantly, for most parameter combinations, the uncoupled model experiences channelization substantially earlier than the coupled model, as seen in Figure 6a. Thus, an important difference that follows from full coupling between hydrology and ice dynamics is not just a reduced speedup but also a longer time until the onset of channelization.

5.5. Parameter Sensitivity of Coupled Feedbacks - Basal Friction Law Parameters

Feedback strength shows a similar range of parameter sensitivity for the basal friction law parameters (Figure 9). C, the Coulomb friction coefficient, controls the relationship between effective pressure and basal traction in the Coulomb region of the friction law parameter space, and $\frac{\lambda_{max}}{m_{max}}$, the wavelength and maximum slope of the dominant bedrock bumps, controls at what value of effective pressure the friction law transitions from the Coulomb region to the nonlinear viscous region. Because the friction law parameters have a strong affect on ice dynamics, the initial speed prior to moulin activation is very sensitive to the parameter values chosen. We restrict our analysis to initial speeds at the moulin site that vary within about an order of magnitude from the base case (see green contour lines on Figure 9).

Interestingly, despite the wide variation in initial speed, there is only small variability in the meltwater input required to achieve the target 4.55× speedup; the required moulin input only varies within an order of magnitude for the friction law parameters sampled. This is opposite from variations in the hydrology parameters, which had similar initial speeds but required vastly different meltwater inputs to achieve the desired speedup. Also in contrast to variations in the hydrology parameters, the dissipation factor, D_f, is insensitive to variations in the friction law; nowhere in the friction law parameter space sampled is the channelization threshold surpassed during spinup.

Interpreting the patterns in friction law parameter sensitivity is more complicated, but a consistent finding is that for a given value of initial speed (along the green contours in Figure 9), the feedback strength decreases (colors trend from blue to red) with larger values of both friction law parameters. The effect of increasing both of these parameters together is to create a narrower, but more sensitive, range of effective pressure values that fall within the Coulomb friction region of the basal friction law. This generates a more localized speedup from a point source of meltwater input, because the transition to the Coulomb friction region of the friction law occurs at lower effective pressure (which translates spatially as only close to the moulin). The more localized speedup has two effects on coupling between hydrology and ice dynamics: (1) with an uncoupled model the ice dynamics forcing to the hydrology model is substantially incorrect only close to the moulin, and (2) larger horizontal gradients in speed near the moulin result in larger horizontal strain rates, more strain softening of the ice causing faster creep closure of cavities, and a stronger positive feedback. Both of these effects minimize the dominant negative feedback associated with sliding opening of

subglacial cavities when the friction law parameters are both large. At large values of the friction law parameters (to the right of the white dashed line in Figure 9), overpressure is required to attain the target speedup; so our model may not be appropriate in this region.

Similar to what was observed when varying the hydrology model parameters, the time to channelization is consistently longer with the coupled model than with the uncoupled model. The longest times to channelization are seen when C is large and $\frac{\lambda_{max}}{m_{max}}$ is small. This corresponds to the magnitude of meltwater input required to achieve the target speedup; smaller inputs result in a longer time to channelization, as expected.

6. Discussion

6.1. Comparison to Observations

The time series of speed associated with our simulated meltwater-induced speedup events bears strong resemblance to the seasonal pattern of surface speed observed on mountain glaciers: the initiation of surface meltwater input to the bed triggers a manyfold increase in surface speed (a spring speedup) that gradually reduces to a late summer speed that is slightly lower than the winter speed. Similarly sized melt inputs later in the summer have a smaller impact on the velocity. The ability of our coupled model to reproduce this qualitative behavior is not surprising—previous similar studies have demonstrated the same result [*Pimentel and Flowers*, 2010; *Hewitt*, 2013] and the subglacial hydrology model was designed to include the relevant processes.

In this study, however, we emphasize the role of the evolution of the capacity of the distributed system and feedbacks between the distributed system and ice dynamics in the reduction of the initial speedup. A reduction of enhanced sliding despite the continued input of meltwater during a spring speedup is commonly attributed to channelization. However, even without allowing for channelization, substantial reductions in speed occur in our simulations. With one-way forcing (run 1N, Figure 4, black line), water pressure and speed lower over time simply due to the growth of cavity space. When coupling of velocity is included, further reduction of water pressure and speed occur (~25% of the initial speedup) before channelization initiates (Figure 4, red and blue lines). The importance of the evolution of the distributed system in mitigating the initial speedup, particularly when coupling between the hydrology and ice dynamics is included, is a key result of this study.

Nonetheless, the inclusion of channelization in the model produces a speedup event that more closely resembles an observed spring speedup. With the channel present, the rate of slowdown increases over time and a new steady state configuration is quickly reached, whereas without the channel, it takes ~0.5 year for the system to evolve to a new steady state. Importantly, the new steady state sliding speed with the channel is slower than the initial preevent speed. This is analogous to the late summer slowdown observed on mountain glaciers [e.g., *MacGregor et al.*, 2005].

On Haut Glacier d'Arolla (2.2 km long tongue, 130 m thick ice along centerline), *Mair et al.* [2003] observed spring speedups that were approximately fivefold (~7 m yr^{-1} to ~35 m yr^{-1}) in two different years. On Bench Glacier (7 km long, maximum ice thickness 185 m), *MacGregor et al.* [2005] observed spring speedups that were twofold to fivefold in two different years. The sizes of these glaciers and the spring speedup magnitude are both roughly similar to what we model here. Additionally, the sliding speeds and proglacial discharge of our spun-up initial state (Figures 2c and 2d) are roughly consistent with observations on these glaciers. The modeled water flux across the terminus (0.24 m^3 s^{-1}) is comparable in magnitude to the early season proglacial discharge (~1 m^3 s^{-1}) observed by *Mair et al.* [2003] and *MacGregor et al.* [2005].

However, termination of spring speedup on both glaciers is ~5–20 days, whereas in our simulations that include channelization, it is ~60 days before surface velocities return to initial values (Figure 6). We have made no attempt to deliberately model a specific glacier, and therefore, the mismatch in duration of speedup may simply result from improper geometry or parameter choices. Furthermore, our sustained steady input of surface meltwater is unrealistic. In the real-world observations referenced above, the elevated temperature and/or precipitation events associated with the initial spring speedup are short-lived themselves; part or all of the termination of the initial speedup in those cases may be due to the temporary cessation or reduction of surface meltwater inputs to the bed. Similarly, the existence of a single moulin in our experiments unrealistically limits the delivery of meltwater to the bed, which certainly delays channelization. Finally, our model does not include the possibility of preferential subglacial flow paths due to

partially open conduits or zones of higher hydraulic conductivity [*Gulley et al.*, 2012] which would allow channels to evolve more rapidly than shown here. Indeed, Haut Glacier d'Arolla is believed to contain a zone of high hydraulic conductivity where fine material has been flushed from basal sediments through repeated occupation by large channels [*Hubbard et al.*, 1995].

6.2. Importance of Feedbacks in the Coupled System

In section 4, we identified three feedbacks in the coupled system: sliding-opening of cavities (negative), melting associated with frictional heat from sliding (positive), and strain softening of basal ice (positive). For this test case, we find that only the negative, sliding-opening feedback is important (Figure 4). As stated, a substantial fraction of the reduction in speedup for our base case is due to this negative feedback (Figure 4). Across almost the entirety of parameter space we sampled, the net feedback is negative at all times (only 3% of parameter combinations sampled ever exhibit a net positive feedback), with the sliding-opening feedback reducing transient speeds to less than half the speeds generated by one-way forcing in some cases (Figures 8–9).

The other two feedbacks are insignificant for this test case. In addition to opening cavities, increased sliding can also generate additional basal melt through frictional heating (if basal traction is reduced enough, frictional heating can actually decrease or vanish during a speedup event, but here we find it typically increases). For this test case, the locally increased frictional melt during speedup is larger than melt from the geothermal flux, but ~3 orders of magnitude smaller than the moulin input. In other words, frictional heating changes local basal melting substantially, but basal melt remains insignificant compared to surface meltwater inputs. For smaller moulin inputs, frictional melt generation may be more important, but its impact is probably typically dwarfed by the opening of cavities by sliding, as reported by *Bartholomaus et al.* [2011] for a modeling application to Kennicott Glacier, Alaska. The strain-softening feedback is small but noticeable when only effective ice viscosity is coupled between the hydrology and ice dynamics models. However, when both sliding and viscosity are coupled, the effects of the strain-softening feedback become negligible for most parameter combinations, again due to the strength of the sliding-opening feedback.

The importance of the sliding-opening feedback has been identified by some observational studies. The retardation of sliding by cavity growth has been proposed to explain observations of speed on Findelengletscher, Switzerland [*Iken and Truffer*, 1997], and Kennicott Glacier, Alaska [*Bartholomaus et al.*, 2011]. *Iken and Truffer* [1997] discuss the possibility of how the passive opening of isolated cavities responding to changes in pressure and sliding in the interconnected cavity system would have a regulating effect on the overall basal traction. We have not considered isolated cavities, but this effect is consistent with our results. Finally, on Bench Glacier, Alaska, a model that included opening of cavities through sliding reproduced observed surface uplift during the first part of the summer prior to the formation of channels [*Anderson et al.*, 2004], consistent with the findings here that cavity opening is a key process prior to channelization.

While we see widespread importance of this feedback across the range of parameter values considered, it is unknown how universally these results extend to other glacier geometries (e.g., thicker ice and flatter slopes) and to other forcings. Particularly, a more realistic diurnally varying melt input may reveal a different degree of importance for the sliding-opening feedback. Previous modeling studies have found that the differences in water pressure generated by diurnally varying forcing and daily averaged forcing are small when averaged over daily time scales [*Hewitt*, 2013; *Werder et al.*, 2013]. While there is reason to believe that the nonlinear nature of the basal friction law used here (and other commonly used power law friction laws) could generate substantially different velocities and net displacement with diurnal inputs than with steady inputs [*Schoof*, 2010; *Werder et al.*, 2013], *Hewitt* [2013] found similar daily mean velocity with both types of forcing. We expect that feedback strength is not strongly affected by diurnally varying inputs because the largest feedback effects are associated with the cumulative change in distributed system capacity (increase in layer thickness), but diurnal forcing may impact time to channelization.

6.3. Model Limitations

While our model results produce realistic behavior, there are a number of areas that warrant further investigation. There is a general uncertainty in the functional form of the opening and closing terms of the distributed (equation (2)) and channel (equation (11)) models, as well as the choice of water flow law(s) (equations (6) and (13)). While various choices of parametrizations for each component of the hydrology

model can simply be swapped into this model framework as is appropriate for a particular application, the appropriate choice is rarely known due to the difficulty in making direct observations at the glacier bed.

The opening of channels is on the strongest theoretical foundation, but there is substantial uncertainty regarding the details of the opening of the distributed system. The simple linear relationship used here (equation (3)) certainly captures the important qualitative features of the relationship, but a more sophisticated relationship can be applied if, for example, more is known or assumed about the geometry of bedrock bumps [e.g., *Kamb*, 1987; *Anderson et al.*, 2004]. Additionally, inclusion of opening of cavities through melting may be appropriate in some circumstances. As argued in the Appendix, this should be considered carefully, as it can have a strong impact on the modeled water pressure.

Similarly, while we have used a linear relation between effective pressure and creep closure for simplicity, which, again, captures the general qualitative nature of the relationship, a cubic relationship [e.g., *Schoof et al.*, 2012; *Hewitt*, 2013; *Werder et al.*, 2013] would be more consistent with the constitutive relationship assumed by the ice dynamics model. A shape factor can also be incorporated into the creep closure relationship if something is known or assumed about the specific shape of cavities and channels.

The proper choice of flow law in the hydrology model is unclear, with various authors using relations describing both laminar and turbulent flow. We note an interesting feature with the distributed flow relation used here (equation (6)). The cubic dependence of flux on sheet thickness requires very small bump heights ($<\sim$8 cm, Figure 8) in order to avoid channelization at steady state even without surface meltwater inputs (because the critical discharge is quickly reached if water depth is allowed to be larger). This may be a limitation of the model because it is generally assumed that channels completely close down over winter and it is reasonable to expect larger bump heights on some glaciers. (However, there is evidence that channels persist during extended periods without meltwater input (i.e., winter) on some glaciers [e.g., *Gulley et al.*, 2012].)

In addition to these uncertainties in the model formulation, the model we present here has limitations that may make it inappropriate for certain problems. Conditions of overpressure and underpressure are not handled accurately, and such conditions can be common during spring speedup and fall shutdown, respectively, particularly where glacier slopes vary dramatically (e.g., overdeepenings, riegels, and near margins) [*Schoof et al.*, 2012]. Also, our model does not include a storage term which can have a large impact on the transient response of the hydrologic system by damping oscillations (particularly those associated with diurnal variations in meltwater input) and reducing effects of the channel on the distributed system [*Werder et al.*, 2013; *Hewitt*, 2013; *Bartholomaus et al.*, 2011]. Finally, though we are applying the coupled model to transient events, the Coulomb friction law used here (equation (20)) is based on steady state assumptions of cavitation [*Schoof*, 2005]. At present there is not a more rigorous solution to this problem, but additional work may offer a basal friction law that includes the effects of changing cavity size, which would allow complete consistency between the basal hydrology and basal friction formulations [*Hewitt*, 2013; *Iken*, 1981; *Howat et al.*, 2008].

Despite these limitations and uncertainties, the major finding of this study, that sliding-opening of cavities is an important negative feedback in distributed drainage systems, should be robust regardless of the specific parameterizations used for various processes and specific glacier geometry considered. The relative strength of this feedback will, of course, vary, but it is driven by the importance of cavity opening in distributed drainage [e.g., *Walder*, 1986]. Nonetheless, we stress that results will vary quantitatively with different model formulations, and we expect feedback strength to be most sensitive to the formulation used for the opening term (equation (3)).

As for the effect of glacier geometry on these results, we again expect the major finding to be robust, with some caveats. Close to glacier margins, dynamics of both the water and ice systems are strongly controlled by boundary effects, which may overshadow some of the processes found to be dominant here. For ice sheet geometries with thicker ice, lower surface slopes, and faster sliding speeds, we hypothesize that the sliding-opening feedback would remain important. Feedback strength scales with relative speedup (as opposed to absolute speedup); while speeds on the Greenland Ice Sheet are typically many times larger than for the idealized glacier modeled here, similar speedups (twofold to fivefold) are commonly observed [e.g., *Hoffman et al.*, 2011]. One difference likely to be important in interior ice sheet settings is the low surface slopes that appear to delay or prevent channelization [*Meierbachtol et al.*, 2013]. This would allow for greater time periods over which feedbacks within the distributed drainage system could operate.

7. Conclusions

We have coupled a two-dimensional subglacial hydrology model that includes distributed and channelized drainage with a three-dimensional higher order ice dynamics model in order to explore feedbacks between the two systems for hard-bedded glaciers. We identified one negative feedback, sliding-opening of cavities, and two positive feedbacks, sliding-induced basal melt and strain softening of basal ice. Only the sliding-opening feedback is important in our experiments, and it is substantial across the range of parameter values explored.

Notably, evolution of the distributed hydrologic system, particularly when the sliding-opening feedback is included, can qualitatively act (and thus observationally "look") like channelization; a reduction in water pressure and associated sliding occurs with steady meltwater inputs. Evolution of the distributed hydrologic system occurs much more slowly than channelization, but a substantial period of time can pass and a substantial fraction of recovery from a speedup event can occur as a result, prior to channel initiation. Nevertheless, we find that channelization is required to both terminate a meltwater-induced speedup event over appropriate timescales (i.e., before the end of summer) and to obtain a late summer slowdown commensurate with observations. In our simulations, feedbacks between the subglacial hydrology and ice dynamics cease to become important once channelization begins.

Our results argue that a coupled treatment of subglacial hydrology and ice dynamics is required to fully represent evolution of a subglacial hydrologic system composed of distributed drainage only. These conditions are common when surface meltwater inputs are low, including mountain glaciers during winter and the initial phases of spring speedup. This also applies to the ablation zone of the Greenland ice sheet where smaller hydraulic gradients associated with flatter slopes may help to delay channelization [*Meierbachtol et al.*, 2013].

Appendix A: Role of Melt Opening in Distributed Drainage

While opening of channels through melting is a fundamental process for channel evolution, the role of basal melting in evolution of the distributed system is less clear. Heat for melting of basal ice can come from three sources: the geothermal heat flux, friction from sliding of the ice over the basal substrate, and viscous dissipation within the water flow (the pressure dependence of the melting temperature also affects the sensible heat of the water, but we have not considered that here).

If melting is spatially uniform across areas of the glacier sole in contact with both bumps and cavities, basal melt will result in no enlargement of cavities, because the glacier will simply lower uniformly, supported by the highest supporting bumps [*Creyts and Schoof*, 2009]. In this case, the production of basal melt is equivalent to the addition of surface melt—the addition of water without the addition of cavity space—which increases water pressure.

Assuming instantaneous mixing of heat within subglacial water and water-filled cavities (which we restrict ourselves to in our model formulation), a uniform basal heat flux will result in uniform basal melting. In contrast, frictional heat generated from sliding of the ice will be concentrated where the ice contacts its substrate—along the top and stoss sides of bumps. Thus, melting associated with heat from sliding may actually generate melt while *reducing* spatially averaged cavity space. For simplicity, in our model we treat melt from both geothermal heat and frictional heat as water sources that do not affect cavity space (and therefore are not appropriate as an opening mechanism in equation (2)), but a more complicated treatment of sliding-generated heat could be made if the details of ice-bed contact geometry were established.

If basal melt is concentrated away from the bumps supporting the ice (i.e., within the cavities), then melting will add both water and cavity space. However, due to the difference in density between water and ice, more cavity space will be added than water, which results in a lowering of water pressure. The only heat source that will be localized away from supporting bumps is viscous dissipation of the water flow. We have deliberately chosen to avoid including this heating term in the distributed system due to its eventual instability [*Walder*, 1986; *Kamb*, 1987; *Hewitt*, 2011; *Schoof*, 2010] but indirectly account for it by allowing channelization to occur when this term would become the dominant opening mechanism (equation (9)).

Thus, we argue that under most circumstances, including a melt opening term due to geothermal or sliding heat in the evolution of the distributed system (equation (2)) is not appropriate from geometric

considerations. (As discussed above and by *Schoof et al.* [2012], *Hewitt* [2013], and *Werder et al.* [2013], it is generally desirable to exclude viscous dissipation from the distributed system to avoid instability but include the associated melt flux in the channelized system in some way.) From a practical perspective, we find that choosing to include opening of cavities from basal melt leads to unrealistically low, or even negative, water pressure in some situations. For example, if melt opening is allowed in the spinup of the primary experiment discussed above, the water pressure as a fraction of overburden is 54% versus 59% when we exclude it. Field observations of borehole water pressure prior to spring speedup are commonly 60–100% [e.g., *Iken and Bindschadler*, 1986; *Hooke and Pohjola*, 1994; *Kavanaugh and Clarke*, 2001; *Harper et al.*, 2002; *Kavanaugh*, 2009].

Acknowledgments

This work was supported by Climate Modeling Programs within the U.S. Department of Energy Office of Science and by the National Science Foundation, under grant ANT-0424589 to the Center for Remote Sensing of Ice Sheets (CReSIS). We thank Mauro Werder, Ian Hewitt, Tim Creyts, Christian Schoof, Gwenn Flowers, and Jesse Johnson for enlightening discussions on subglacial hydrology and model formulation. Conversations with Douglas Jacobsen and Jeremy Fyke aided model development and analysis. Reviews by Martin Truffer and two anonymous reviewers contributed very valuable feedback that improved the manuscript. Finally, we thank Associate Editor Erin Pettit and Editor Bryn Hubbard for their editorial guidance.

References

Alley, R. (1989), Water-pressure coupling of sliding and bed deformation: I. Water system, *J. Glaciol.*, *35*(119), 108–118.

Amundson, J. M., M. Truffer, M. P. Lu, and C. Zu (2006), Time-dependent basal stress conditions beneath Black Rapids Glacier, Alaska, USA, inferred from measurements of ice deformation and surface motion, *J. Glaciol.*, *52*(178), 347–357.

Anderson, R. S., S. P. Anderson, K. R. MacGregor, E. D. Waddington, S. O'Neel, C. A. Riihimaki, and M. G. Loso (2004), Strong feedbacks between hydrology and sliding of a small Alpine glacier, *J. Geophys. Res.*, *109*(F3), F03005, doi:10.1029/2004JF000120.

Arnold, N., and M. Sharp (2002), Flow variability in the Scandinavian ice sheet: Modelling the coupling between ice sheet flow and hydrology, *Quat. Sci. Rev.*, *21*, 485–502.

Banwell, A. F., I. C. Willis, and N. S. Arnold (2013), Modelling subglacial water routing at Paakitsoq, W Greenland, *J. Geophys. Res. Earth Surf.*, *118*, 1282–1295, doi:10.1002/jgrf.20093.

Bartholomaus, T. C., R. S. Anderson, and S. P. Anderson (2008), Response of glacier basal motion to transient water storage, *Nat. Geosci.*, *1*(1), 33–37, doi:10.1038/ngeo.2007.52.

Bartholomaus, T. C., R. S. Anderson, and S. P. Anderson (2011), Growth and collapse of the distributed subglacial hydrologic system of Kennicott Glacier, Alaska, USA, and its effects on basal motion, *J. Glaciol.*, *57*(206), 985–1002, doi:10.3189/002214311798843269.

Bartholomew, I., P. Nienow, D. Mair, A. Hubbard, M. A. King, and A. Sole (2010), Seasonal evolution of subglacial drainage and acceleration in a Greenland outlet glacier, *Nat. Geosci.*, *3*, 408–411, doi:10.1038/NGEO863.

Bartholomew, I., P. Nienow, A. Sole, D. Mair, T. Cowton, and M. a. King (2012), Short-term variability in Greenland Ice Sheet motion forced by time-varying meltwater drainage: Implications for the relationship between subglacial drainage system behavior and ice velocity, *J. Geophys. Res.*, *117*(F3), F03002, doi:10.1029/2011JF002220.

Bell, R. E. (2008), The role of subglacial water in ice-sheet mass balance, *Nat. Geosci.*, *1*(5), 297–304, doi:10.1038/ngeo186.

Blatter, H. (1995), Velocity and stress-fields in grounded glaciers—A simple algorithm for including deviatoric stress gradients, *J. Glaciol.*, *41*(138), 333–344.

Bougamont, M., S. Price, P. Christoffersen, and a. J. Payne (2011), Dynamic patterns of ice stream flow in a 3-D higher-order ice sheet model with plastic bed and simplified hydrology, *J. Geophys. Res.*, *116*(F4), F04018, doi:10.1029/2011JF002025.

Clarke, G. K. (2005), Subglacial processes, *Annu. Rev. Earth Planet. Sci.*, *33*(1), 247–276, doi:10.1146/annurev.earth.33.092203.122621.

Colgan, W., H. Rajaram, R. Anderson, K. Steffen, T. Phillips, I. Joughin, H. J. Zwally, and W. Abdalati (2011), The annual glaciohydrology cycle in the ablation zone of the Greenland ice sheet: Part 1. Hydrology model, *J. Glaciol.*, *57*(204), 697–709, doi:10.3189/002214311797409668.

Creyts, T. T., and C. G. Schoof (2009), Drainage through subglacial water sheets, *J. Geophys. Res.*, *114*(F4), F04008, doi:10.1029/2008JF001215.

Cuffey, K. M., and W. S. B. Paterson (2010), *The Physics of Glaciers*, 693 pp. 4th ed., Elsevier, Amsterdam.

Dukowicz, J. K., S. F. Price, and W. H. Lipscomb (2010), Consistent approximations and boundary conditions for ice-sheet dynamics from a principle of least action, *J. Glaciol.*, *56*(197), 480–496, doi:10.3189/002214310792447851.

Evans, K. J., et al. (2012), A modern solver interface to manage solution algorithms in the Community Earth System Model, *Int. J. High Perform. Comput. Appl.*, *26*(1), 54–62, doi:10.1177/1094342011435159.

Flowers, G. E. (2002a), A multicomponent coupled model of glacier hydrology 1. Theory and synthetic examples, *J. Geophys. Res.*, *107*(B11), 2287, doi:10.1029/2001JB001122.

Flowers, G. E. (2002b), A multicomponent coupled model of glacier hydrology 2. Application to Trapridge Glacier, Yukon, Canada, *J. Geophys. Res.*, *107*(B11), 2288, doi:10.1029/2001JB001124.

Flowers, G. E. (2008), Subglacial modulation of the hydrograph from glacierized basins, *Hydrol. Processes*, *22*(19), 3903–3918, doi:10.1002/hyp.7095.

Fountain, A. G., and J. S. Walder (1998), Water flow through temperate glaciers, *Rev. Geophys.*, *36*(3), 299–328.

Gagliardini, O., D. Cohen, P. Råback, and T. Zwinger (2007), Finite-element modeling of subglacial cavities and related friction law, *J. Geophys. Res.*, *112*(F2), F02027, doi:10.1029/2006JF000576.

Gillet-Chaulet, F., O. Gagliardini, H. Seddik, M. Nodet, G. Durand, C. Ritz, T. Zwinger, R. Greve, and D. G. Vaughan (2012), Greenland ice sheet contribution to sea-level rise from a new-generation ice-sheet model, *The Cryosphere*, *6*(6), 1561–1576, doi:10.5194/tc-6-1561-2012.

Gladish, C. V., D. M. Holland, P. R. Holland, and S. F. Price (2012), Ice-shelf basal channels in a coupled ice/ocean model, *J. Glaciol.*, *58*(212), 1527–1544, doi:10.3189/2012JoG12J003.

Goeller, S., M. Thoma, K. Grosfeld, and H. Miller (2013), A balanced water layer concept for subglacial hydrology in large-scale ice sheet models, *Cryosphere*, *7*(4), 1095–1106, doi:10.5194/tc-7-1095-2013.

Gulley, J., M. Grabiec, J. Martin, J. Jania, G. Catania, and P. Glowacki (2012), The effect of discrete recharge by moulins and heterogeneity in flow-path efficiency at glacier beds on subglacial hydrology, *J. Glaciol.*, *58*(211), 926–940, doi:10.3189/2012JoG11J189.

Harper, J. T., N. F. Humphrey, and M. C. Greenwood (2002), Basal conditions and glacier motion during the winter/spring transition, Worthington Glacier, Alaska, U.S.A., *J. Glaciol.*, *48*(160), 42–50.

Herterich, K. (1987), On the flow within the transition zone between ice sheet and ice shelf, in *Dynamics of the West Antarctic Ice Sheet, Glaciology and Quaternary Geology*, vol. 4, edited by C. van der Veen, and J. Oerlemans, pp. 185–202, Springer, Netherlands. doi:10.1007/978-94-009-3745-1_11.

Hewitt, I., C. Schoof, and M. Werder (2012), Flotation and free surface flow in a model for subglacial drainage. Part 2. Channel flow, *J. Fluid Mech.*, *702*, 157–187.

Hewitt, I. J. (2011), Modelling distributed and channelized subglacial drainage: The spacing of channels, *J. Glaciol.*, *57*(202), 302–314, doi:10.3189/002214311796405951.

Hewitt, I. J. (2013), Seasonal changes in ice sheet motion due to melt water lubrication, *Earth Planet. Sci. Lett.*, *371*, 16–25, doi:10.1016/j.epsl.2013.04.022.

Hoffman, M. J., G. A. Catania, T. A. Neumann, L. C. Andrews, and J. A. Rumrill (2011), Links between acceleration, melting, and supraglacial lake drainage of the western Greenland Ice Sheet, *J. Geophys. Res.*, *116*(F4), F04035, doi:10.1029/2010JF001934.

Hooke, R. L., and V. A. Pohjola (1994), Hydrology of a segment of a glacier situated in an overdeepening, Storglaciären, Sweden, *J. Glaciol.*, *40*(134), 140–148.

Howat, I. M., S. Tulaczyk, E. Waddington, and H. Björnsson (2008), Dynamic controls on glacier basal motion inferred from surface ice motion, *J. Geophys. Res.*, *113*(F3), F03015, doi:10.1029/2007JF000925.

Hubbard, B., M. Sharp, I. Willis, M. Nielsen, and C. Smart (1995), Borehole water-level variations and the structure of the subglacial hydrological system of Haut Glacier d'Arolla, Valais, Switzerland, *J. Glaciol.*, *41*(139), 572–583.

Humphrey, N. F. (1987), Coupling between water pressure and basal sliding in a linked-cavity hydraulic system, in *The Physical Basis of Ice Sheet Modelling (Proceedings of the Vancouver Symposium, August 1987)*, vol. 170, edited by E. D. Waddington and J. S. Walder, pp. 105–119, IAHS Press, Oxfordshire OX108BB, U. K.

Iken, A. (1981), The effect of the subglacial water pressure on the sliding velocity of a glacier in an idealized numerical model, *J. Glaciol.*, *27*(97), 407–421.

Iken, A., and R. A. Bindschadler (1986), Combined measurements of subglacial water pressure and surface velocity of the Findelengletscher, Switzerland: Conclusions about drainage system and sliding mechanism, *J. Glaciol.*, *32*(110), 101–119.

Iken, A., and M. Truffer (1997), The relationship between subglacial water pressure and velocity of Findelengletscher, Switzerland, during its advance and retreat, *J. Glaciol.*, *43*(144), 328–338.

Iken, A., H. Röthlisberger, A. Flotron, and W. Haeberli (1983), The uplift of Unteraargletscher at the beginning of the melt season—A consequence of water storage at the bed?, *J. Glaciol.*, *29*(101), 28–47.

Johnson, J., and J. L. Fastook (2002), Northern Hemisphere glaciation and its sensitivity to basal melt water, *Quat. Int.*, *95-96*, 65–74, doi:10.1016/S1040-6182(02)00028-9.

Kamb, B. (1987), Glacier surge mechanism based on linked cavity configuration of the basal water conduit system, *J. Geophys. Res.*, *92*(B9), 9083–9100.

Kavanaugh, J. L. (2009), Exploring glacier dynamics with subglacial water pressure pulses: Evidence for self-organized criticality?, *J. Geophys. Res.*, *114*(F1), F01021, doi:10.1029/2008JF001036.

Kavanaugh, J. L., and G. K. C. Clarke (2001), Abrupt glacier motion and reorganization of basal shear stress following the establishment of a connected drainage system, *J. Glaciol.*, *47*(158), 472–480.

Kessler, M. a., and R. S. Anderson (2004), Testing a numerical glacial hydrological model using spring speed-up events and outburst floods, *Geophys. Res. Lett.*, *31*(18), L18503, doi:10.1029/2004GL020622.

Kyrke-Smith, T. M., R. F. Katz, and A. C. Fowler (2014), Subglacial hydrology and the formation of ice streams, *Proc. Phys. Soc. London, Sect. A*, *470*, 20,130,494, doi:10.1098/rspa.2013.0494.

Larour, E., H. Seroussi, M. Morlighem, and E. Rignot (2012), Continental scale, high order, high spatial resolution, ice sheet modeling using the Ice Sheet System Model (ISSM), *J. Geophys. Res.*, *117*(F1), F01022, doi:10.1029/2011JF002140.

Le Brocq, A., A. Payne, M. Siegert, and R. Alley (2009), A subglacial water-flow model for West Antarctica, *J. Glaciol.*, *55*(193), 879–888, doi:10.3189/002214309790152564.

Lemieux, J.-F., S. F. Price, K. J. Evans, D. Knoll, A. G. Salinger, D. M. Holland, and A. J. Payne (2011), Implementation of the Jacobian-free Newton–Krylov method for solving the first-order ice sheet momentum balance, *J. Comput. Phys.*, *230*(17), 6531–6545, doi:10.1016/j.jcp.2011.04.037.

Leng, W., L. Ju, M. Gunzburger, S. Price, and T. Ringler (2012), A parallel high-order accurate finite element nonlinear Stokes ice sheet model and benchmark experiments, *J. Geophys. Res.*, *117*, F01001, doi:10.1029/2011JF001962.

Lipscomb, W., R. Bindschadler, S. Price, E. Bueler, J. Johnson, and D. Holland (2009), A community ice sheet model for sea level prediction, *Eos, Trans. AGU*, *90*(3), 23, doi:10.1029/2009EO030004.

Little, C. M., et al. (2007), Toward a new generation of ice sheet models, *Eos, Trans. AGU*, *88*(52), 578–579, doi:10.1029/2007EO520002.

Lüthi, M., M. Funk, A. Iken, S. Gogineni, and M. Truffer (2002), Mechanisms of fast flow in Jakobshavn Isbrae, West Greenland: Part III. Measurements of ice deformation, temperature and cross-borehole conductivity in boreholes to the bedrock, *J. Glaciol.*, *48*(162), 369–385.

MacGregor, K. R., C. A. Riihimaki, and R. S. Anderson (2005), Spatial and temporal evolution of rapid basal sliding on Bench Glacier, Alaska, USA, *J. Glaciol.*, *51*(172), 49–63.

Mair, D., P. Nienow, M. J. Sharp, T. Wohlleben, and I. Willis (2002), Influence of subglacial drainage system evolution on glacier surface motion : Haut Glacier d'Arolla, Switzerland, *J. Geophys. Res.*, *107*(B8), EPM 8-1–EPM 8-13, doi:10.1029/2001JB000514.

Mair, D., I. Willis, U. H. Fischer, B. Hubbard, P. Nienow, and A. Hubbard (2003), Hydrological controls on patterns of surface, internal and basal motion during three "spring events": Haut Glacier d'Arolla, Switzerland, *J. Glaciol.*, *49*(167), 555–567.

Marshall, S. J., H. Björnsson, G. E. Flowers, and G. Clarke (2005), Simulation of Vatnajökull ice cap dynamics, *J. Geophys. Res.*, *110*(F3), F03009, doi:10.1029/2004JF000262.

Meierbachtol, T., J. Harper, and N. Humphrey (2013), Basal drainage system response to increasing surface melt on the Greenland Ice Sheet, *Science*, *341*(6147), 777–779.

Nienow, P., M. Sharp, and I. Willis (1998), Seasonal changes in the morphology of the subglacial drainage system, Haut Glacier d'Arolla, Switzerland, *Earth Surf. Processes Landforms*, *23*(9), 825–843, doi:10.1002/(SICI)1096-9837(199809)23:9<825::AID-ESP893>3.0.CO;2-2.

Nye, J. F. (1951), The flow of glaciers and ice-sheets as a problem in plasticity, *Proc. R. Soc. London, Ser. A*, *207*(1091), 554–572.

Nye, J. F. (1976), Water flow in glaciers: JÖKulhlaups, tunnels and veins, *J. Glaciol.*, *17*(76), 181–207.

Pattyn, F. (2003), A new three-dimensional higher-order thermomechanical ice sheet model: Basic sensitivity, ice stream development, and ice flow across subglacial lakes, *J. Geophys. Res.*, *108*(B8), 2382, doi:10.1029/2002JB002329.

Pattyn, F., et al. (2008), Benchmark experiments for higher-order and full-Stokes ice sheet models (ISMIPHOM), *Cryosphere*, *2*(2), 95–108, doi:10.5194/tc-2-95-2008.

Perego, M., M. Gunzburger, and J. Burkardt (2012), Parallel finite-element implementation for higher-order ice-sheet models, *J. Glaciol.*, *58*(207), 76–88, doi:10.3189/2012JoG11J063.

Pimentel, S., and G. E. Flowers (2010), A numerical study of hydrologically driven glacier dynamics and subglacial flooding, *Proc. R. Soc. London, Ser. A*, *467*(2126), 537–558, doi:10.1098/rspa.2010.0211.
Pimentel, S., G. E. Flowers, and C. G. Schoof (2010), A hydrologically coupled higher-order flow-band model of ice dynamics with a Coulomb friction sliding law, *J. Geophys. Res.*, *115*(F4), F04023, doi:10.1029/2009JF001621.
Price, S., G. Flowers, and C. Schoof (2011a), Improving hydrology in land ice models, *Eos Trans. AGU*, *92*(19), 164.
Price, S. F., A. J. Payne, I. M. Howat, and B. E. Smith (2011b), Committed sea-level rise for the next century from Greenland ice sheet dynamics during the past decade, *PNAS*, *108*(22), 8978–83, doi:10.1073/pnas.1017313108.
Röthlisberger, H., and 1972, Water pressure in intra- and subglacial channels, *J. Glaciol.*, *11*(62), 77–203.
Schoof, C. (2005), The effect of cavitation on glacier sliding, *Proc. R. Soc. London, Ser. A*, *461*(2055), 609–627, doi:10.1098/rspa.2004.1350.
Schoof, C. (2010), Ice-sheet acceleration driven by melt supply variability, *Nature*, *468*, 803–806, doi:10.1038/nature09618.
Schoof, C., I. J. Hewitt, and M. a. Werder (2012), Flotation and free surface flow in a model for subglacial drainage. Part 1. Distributed drainage, *J. Fluid Mech.*, *702*, 126–156, doi:10.1017/jfm.2012.165.
Shannon, S. R., et al. (2013), Enhanced basal lubrication and the contribution of the Greenland ice sheet to future sea-level rise, *PNAS*, *35*(110), 14,156–14,161.
Truffer, M., K. A. Echelmeyer, and W. D. Harrison (2001), Implications of till deformation on glacier dynamics, *J. Glaciol.*, *47*(156), 123–134.
van der Wel, N., P. Christoffersen, and M. Bougamont (2013), The influence of subglacial hydrology on the flow of Kamb Ice Stream, *J. Geophys. Res. Earth Surf.*, *118*, 97–110, doi:10.1029/2012JF002570.
Walder, J. S. (1986), Hydraulics of subglacial cavities, *J. Glaciol.*, *32*(112), 439–445.
Werder, M. A., I. J. Hewitt, C. G. Schoof, and G. E. Flowers (2013), Modeling channelized and distributed subglacial drainage in two dimensions, *J. Geophys. Res. Earth Surf.*, *118*, 2140–2158, doi:10.1002/jgrf.20146.